Journal of Hydrology 639 (2024) 131472

Contents lists available at ScienceDirect

Journal of Hydrology

journal homepage: www.elsevier.com/locate/jhydrol

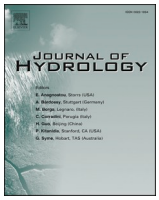

Research papers

Climate and vegetation change impacts on future conterminous United States water yield

Henrique F. Duarte [a,b], John B. Kim [c], Ge Sun [b,*], Steven G. McNulty [b], Jingfeng Xiao [a,*]

[a] Earth Systems Research Center, Institute for the Study of Earth, Oceans, and Space, University of New Hampshire, 8 College Road, Durham, NH 03824, United States
[b] Eastern Forest Environmental Threat Assessment Center, USDA Forest Service, 3041 E. Cornwallis Road, Research Triangle Park, NC 27709, United States
[c] Western Wildland Environmental Threat Assessment Center, USDA Forest Service, 3200 SW Jefferson Way, Corvallis, OR 97331, United States

ARTICLE INFO

This manuscript was handled by Marco Borga, Editor-in-Chief, with the assistance of Hanbo Yang, Associate Editor

Keywords:
Climate change
Dynamic global vegetation model
Evapotranspiration
Hydrology model
Water yield
CONUS

ABSTRACT

Future water availability is influenced by both climate and associated vegetation dynamics. This study coupled vegetation projections from a dynamic global vegetation model (MC2) with an ecohydrological model, Water Supply Stress Index (WaSSI), to predict water yield at the 8-digit Hydrologic Unit Code (HUC8) watershed level for the conterminous United States (CONUS) for the 21st century. We considered two contrasting warming scenarios (Representative Concentration Pathways 8.5 and 4.5) and accounted for simulation uncertainty by using a large ensemble of climate model outputs. The coupled model projects a decrease in water yield across much of CONUS, especially towards end-century (2080–2099) under RCP 8.5 (warmer scenario), reaching up to −30% at the regional level, relative to the 2008–2027 baseline period. Overall, the projected water yield reduction under RCP 8.5 is roughly twice as high as under RCP 4.5. Substantial changes in water yield for watersheds in the central and southeastern United States are expected by mid-century (2040–2059), reaching up to −40% (RCP 4.5) and −75% (RCP 8.5) at at the century's end (2080–2099), relative to 2008–2027, respectively. Climate change, rather than vegetation change, strongly dominates the projected future changes in water yield, with contributions typically one order of magnitude higher. For a small number of watersheds, the effects of vegetation change can mitigate or exacerbate the effects of climate change on water yield. Our simulation results suggest a widespread increase in aridity and evaporative indices and a decrease in soil moisture, especially under RCP 8.5. Our integrated modeling results can inform policy makers and resource development planners quantitative information of future water availability.

1. Introduction

Global water availability is rapidly changing due to climate change and human activities (Heidari et al., 2021a; Song et al., 2023; Sun et al., 2023b; Zhang et al., 2023). Watershed water yield is often used as a surrogate of ecosystem and societal water availability. Water yield is defined as the total water produced as the sum of surface flow, subsurface flow, and baseflow. The mean annual water yield represents the long-term (multi-year) mean difference between precipitation (*P*) and evapotranspiration (ET) within a watershed (Sun et al., 2015a). Precipitation and air temperature are the key climatic drivers of water yield (Duan et al., 2017). Under a warmer climate, the partitioning of precipitation between streamflow (i.e., water yield) and ET is generally expected to shift towards ET (Duan et al., 2017). This would further reduce water yield in watersheds projected to receive less precipitation in the future and offset the increase in water yield for watersheds projected to receive more precipitation. In addition to climatic factors, land cover/land use also directly impacts water yield, given its effects on ET (Hu et al., 2021; Li et al., 2020; Liu et al., 2016; Sun et al., 2015a; Zhang et al., 2024). The interception of precipitation by vegetation and posterior evaporation are directly associated with its leaf area index (LAI), and so are its transpiration losses (Yang et al., 2023). In addition to potential land cover/land use changes projected for the future (e.g., urbanization and agricultural expansion), global vegetation cover in terms of total leaf area, stomatal conductance, leaf phenology, and plant species distribution is expected to respond to future climate change and increasing atmospheric CO_2 and temperature (Gonzalez et al., 2010; Mekonnen and Riley, 2023; Teng et al., 2023). For instance, warmer and CO_2-richer conditions may promote plant growth and lead to increased transpiration due to higher LAI and atmospheric evaporative demand

* Corresponding authors.
E-mail addresses: ge.sun@usda.gov (G. Sun), j.xiao@unh.edu (J. Xiao).

https://doi.org/10.1016/j.jhydrol.2024.131472
Received 6 March 2024; Received in revised form 7 May 2024; Accepted 22 May 2024
Available online 15 June 2024

(Zhang et al., 2023). At the same time, stomatal conductance is generally expected to decrease in response to increasing atmospheric CO_2 (Li et al., 2023; Medlyn et al., 2001), which would downregulate transpiration and contribute to reduced water stress on plants. As global climate change intensifies, shifts in precipitation regimes, increased air temperature, and associated changes in vegetation state and function may substantially impact water yield worldwide (Yang et al., 2023). Potential future reductions in water yield compounded with projected increases in water demand across water use sectors may lead to more severe, frequent, and widespread water shortages, impacting ecosystems and human welfare (Brown et al., 2019; Sun et al., 2008; Warziniack et al., 2022).

Future climate projections from the Coupled Model Intercomparison Project Phase 5 (CMIP5) indicate a substantial increase in surface air temperature in CONUS by the end of the twenty-first century (2070–2099), ranging from 1.3° to 3.7 °C under the Representative Concentration Pathway 4.5 (RCP 4.5, a moderate warming scenario in which anthropogenic greenhouse gas emissions peak at mid-century) and from 3.0° to 6.1 °C under RCP 8.5 (a high warming scenario in which emissions increase throughout the 21st century), relative to 1986–2015 (Hayhoe et al., 2018). Under RCP 8.5, much of CONUS annual mean surface air temperature is projected to permanently depart from its historical variability range in the next couple of decades (2029–2050; Kerns et al., 2016). Surface air temperature projections under different warming scenarios (e.g., RCP 4.5 and 8.5) diverge substantially at mid-century, with high and increasing variability among individual general circulation model (GCM) projections within each scenario (Wuebbles et al., 2014). Winter and spring precipitation is projected to increase by up to 25% in the northern Great Plains, the upper Midwest, and the Northeast, and decrease by up to 25% in the Southwest at end-century under RCP 8.5 (2070–2099 relative to 1986–2015; Hayhoe et al., 2018). The frequency of heavy precipitation events is projected to increase in all regions of CONUS, with end-century increases of about 50–100% under RCP 4.5 and 100–200% under RCP 8.5 relative to historical regional values (Easterling et al., 2017).

Several studies have investigated the impact of climate change on water yield over CONUS using hydrological models and downscaled CMIP5 climate projections (e.g., Duan et al., 2017; Heidari et al., 2021a, 2021b; Mahat et al., 2017; Naz et al., 2016). While the future twenty-first century projections in Naz et al. (2016) and Heidari et al., (2021b; "intermediate" and "wet" GCMs) indicate an overall increase in water yield in CONUS under RCP 8.5, the projections in Heidari et al., (2021a), Heidari et al., (2021b; "dry" GCM), and Mahat et al. (2017) indicate an overall decrease in water yield. The spatial patterns of future water yield change projected by Heidari et al., (2021a), Mahat et al. (2017), and Duan et al. (2017) are in general agreement, showing a reduction in water yield across extensive parts of CONUS, especially in the central U.S., with more accentuated changes under RCP 8.5 compared to RCP 4.5. However, these patterns of change contrast with those projected by Naz et al. (2016), which are generally reversed in sign, showing an increase in water yield across much of CONUS including the central U.S. under RCP 8.5. The variation across the cited studies is associated with different modeling approaches or simulation periods. Modeling approaches have included different hydrological models such as the Variable Infiltration Capacity (VIC; Cherkauer et al., 2003; Liang et al., 1996, 1994) and the Water Supply Stress Index (WaSSI: Caldwell et al., 2012; Sun et al., 2011), and different GCM ensembles and GCM downscaling approaches, such as dynamic and statistical downscaling methods (Bias Correction and Constructed Analog, BCCA, Version 2: USBR, 2013; Multivariate Adaptive Constructed Analogs, MACA: Abatzoglou and Brown, 2012; MACAv2-LIVNEH: Livneh et al., 2013). However, a common denominator across these studies is the assumption of a fixed land cover throughout the twenty-first century simulations, despite the fact that land cover is projected to change in response to climate change and increasing atmospheric CO_2 (Gonzalez et al., 2010; Mekonnen and Riley, 2023; Teng et al., 2023). Empirical studies show that vegetation matters to water balances and water availability at multiple scales (Oudin et al., 2008; Zhang et al., 2001, 2017).

Differently from hydrological models, terrestrial biosphere models (TBMs) can account for biogeochemistry and simulate the water and carbon cycles in a coupled fashion, including land cover dynamics. TBMs with dynamic vegetation modeling capability, also known as dynamic global vegetation models (DGVMs), allow not only the vegetation state (e.g., LAI and biomass) but also the distribution of plant functional types to respond dynamically to climate and atmospheric CO_2, while typical TBMs prescribe the distribution. The added complexity in TBMs and DGVMs, however, comes at the price of being more computationally expensive to run in comparison to simpler hydrological models, hindering their application at the fine spatial resolutions typically desired for hydrological studies, especially for large spatial domains. The dependence on a much higher number of model parameters also makes the calibration of TBMs more challenging. Therefore, a common approach for studies focused on future hydrological projections is the use of relatively simple water-centric models and the assumption of a fixed land cover, as in the studies cited in the paragraph above (Duan et al., 2017; Heidari et al., 2021a, 2021b; Mahat et al., 2017; Naz et al., 2016). However, changes in land cover are expected to play a significant role in the modulation of future water yield. For instance, Sun et al. (2015a) investigated the sensitivity of water yield in response to percent changes in LAI across the CONUS using the WaSSI ecohydrological model. They found an overall increase in water yield in CONUS of 3%, 8%, and 13% associated with LAI decreases of 20%, 50%, and 80%, respectively, and a decrease of 3% associated with an LAI increase of 20%. Bridging between the use of fully-coupled, complex TBMs/DGVMs and relatively simple hydrological models with prescribed vegetation – to enable investigations of the impacts of future climate and vegetation change on water yield at fine spatial resolution over a large spatial domain as CONUS – is yet to be explored.

In this paper, we present results from coupling vegetation projections from the MC2 DGVM (Bachelet et al., 2001; Conklin et al., 2016) with the WaSSI hydrological model (Caldwell et al., 2012; Sun et al., 2011) to project water yield for the CONUS at the USGS 8-digit Hydrologic Unit Code watershed scale (HUC8), comparable in size to counties. Our approach represents a one-way coupling technique, i.e., coupling available future projections of LAI and vegetation type from a DGVM with a hydrological model. WaSSI has been extensively validated for CONUS at multiple scales (USGS 2-digit HUC, HUC2, and overall CONUS: Duan et al., 2017; HUC8: Caldwell et al., 2012; USGS 12-digit HUC, HUC12: Li et al., 2020; Sun et al., 2015b) and MC2 has been tested regionally and globally for climate change studies (Golub et al., 2022; Kim et al., 2018, 2017; Zhou et al., 2019). We drove WaSSI with statistically downscaled future climate projections depicting RCP 4.5 and 8.5 scenarios by 16 CMIP5 GCMs (Localized Constructed Analogs, LOCA; Pierce et al., 2015, 2014). We adopted available vegetation projections made with the MC2 DGVM (EPA, 2017) using the same climate driver (LOCA) for integration with WaSSI. While there has been previous work that present future projections of water yield for CONUS, this study is, to our knowledge, the first to employ an ensemble of future vegetation projections and provide water yield projections at a relatively fine scale (i.e., HUC8 watersheds). Our goal was to investigate potential future changes in climate and vegetation and their impact on water balances (e.g., water yield, ET, soil moisture) in CONUS for the mid-century (ca. 2050) and end-century (ca. 2090) under contrasting warming scenarios (RCP 4.5 and 8.5), taking into consideration the uncertainty arising from GCMs. Our central hypothesis was that climate change significantly alters water balances both directly via changes in air temperature and precipitation and indirectly via climate/CO_2-induced changes in leaf area.

2. Methods

2.1. Study area

We carried out our simulations for the conterminous United States (CONUS) at the HUC8 scale, covering a total of 2099 watersheds with an average area of 3752 km^2 (Fig. 1). In Section 3, our results are presented at the HUC8 scale and summarized at the HUC2 scale, i.e., for each one of the 18 USGS water resources regions in CONUS (Fig. 1).

2.2. WaSSI model description

The Water Supply Stress Index (WaSSI) model uses a simplified water balance approach to simulate the monthly water yield, ET, and soil moisture of each HUC8 watershed in a specified domain (Caldwell et al., 2012; Sun et al., 2011). The model has been well tested in the US (Duan et al., 2019; Li et al., 2020) and globally in Germany (Al-Qubati et al., 2023), China (Liu et al., 2013), Rwanda (Bagstad et al., 2018), and Nepal (Sun et al., 2023a) on water yield and ecosystem productivity.

Soil hydrological processes including infiltration, storage, and drainage are simulated with an algorithm based on the Sacramento Soil Moisture Accounting Model (SAC-SMA, Burnash, 1995; Burnash et al., 1973). Monthly ET is initially estimated with an empirical function of potential evapotranspiration (PET), LAI, and P, derived from eddy-covariance flux measurements at multiple sites (Sun et al., 2011). PET is calculated based on air temperature and the daytime length defined by latitude and day of the year (Hamon, 1963). The final ET estimate is constrained by the available soil moisture. Each watershed is composed by up to 10 land cover types: 1) deciduous forest, 2) evergreen forest, 3) mixed forest, 4) shrubland, 5) grassland, 6) barren land, 7) wetland, 8) water, 9) cropland, and 10) urban. Coverage area fraction, impervious cover fraction, and mean monthly LAI values are assigned to each land cover type, while all land cover types share the same watershed soil properties. WaSSI calculates all water balance components for each land cover type independently, and then integrates the results at the watershed level via area-weighted averaging. The model runs on a monthly time step, and is driven with uniform precipitation and air temperature data for each HUC8 watershed.

For CONUS, surface input data, including soil properties based on the Digital General Soil Map of the US (STATSGO2, NRCS, 2024), land and impervious cover based on the 2006 National Land Cover Database (NLCD; USGS, 2011), and LAI based on 2000–2006 mean monthly MODIS LAI (Zhao et al., 2005), is available at the HUC8 scale. Note that we combine the land cover and LAI datasets with MC2 simulations to project values for 2007–2099 (Sect. 2.4), and that we define 2008–2027 as a "present-day" baseline for comparison with mid- and late-century projections of vegetation and hydrology (Sect. 2.5).

The WaSSI model originally assumes no changes in land cover over the years. Therefore, we adapted the model structure to allow for a dynamic land cover. We also applied a small modification in the code regarding the ET calculation. By default, WaSSI calculates a potential actual evapotranspiration value (ET*, i.e., unconstrained by available soil moisture) as:

$$ET^* = 0.0222PET\ LAI + 0.174P + 0.502PET + 5.31LAI \quad (1)$$

For watersheds located in regions 1, 2, 4, and 5 in the northeastern U.S. (Fig. 1) with more than 20% forest cover, WaSSI calculates ET* as:

$$ET^* = 0.00169PET\ P + 0.4PET + 7.83LAI \quad (2)$$

The alternate formulation (Eq. (2)) is used in WaSSI as it was found to improve ET simulations in those cases, when compared to annual observations of P − water yield. With our implementation of dynamic land cover, WaSSI could potentially switch back and forth over time between the two ET* formulations for a given watershed in those regions. To avoid inconsistencies, we opted to remove the forest cover conditional from the code, but kept the alternate ET* formulation for regions 1, 2, 4, and 5.

2.3. Future climate projections

Statistically downscaled climate projections from 16 CMIP5 general circulation/Earth system models under scenarios RCP 4.5 and 8.5 were used with WaSSI (Localized Constructed Analogs, LOCA: Pierce et al., 2015, 2014; see Table 1). The model/scenario selection was based on the availability of corresponding MC2 simulations (Section 2.4). The near-surface air temperature and precipitation data from the LOCA downscaled climate dataset were aggregated from the original 1/16°, daily

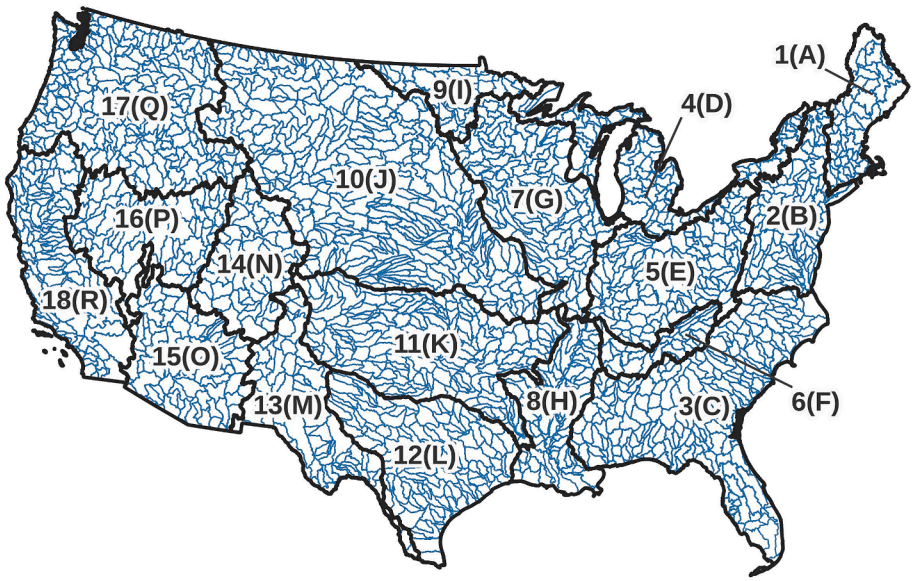

Fig. 1. USGS HUC8 watersheds (blue lines) and HUC2 water resources regions (black lines) in CONUS. Regions include 1) New England, 2) Mid-Atlantic, 3) South Atlantic-Gulf, 4) Great Lakes, 5) Ohio, 6) Tennessee, 7) Upper Mississippi, 8) Lower Mississippi, 9) Souris-Red-Rainy, 10) Missouri, 11) Arkansas-White-Red, 12) Texas-Gulf, 13) Rio Grande, 14) Upper Colorado, 15) Lower Colorado, 16) Great Basin, 17) Pacific Northwest, and 18) California. Corresponding short labels (A to R) are used in the figures in Section 3. (For interpretation of the references to colour in this figure legend, the reader is referred to the web version of this article.)

Table 1
LOCA climate datasets used as input to WaSSI (LOCA statistically downscales CMIP5 model outputs to 1/16° resolution for the conterminous United States; Pierce et al., 2015, 2014).

Model	Institution	Original spatial resolution (*lon* × *lat*)	Reference
ACCESS1-0	Commonwealth Scientific and Industrial Research Organisation, and Bureau of Meteorology, Australia	1.875° × 1.25°	(Bi et al., 2013)
CanESM2	Canadian Centre for Climate Modelling and Analysis	2.8° × 2.8°	(Chylek et al., 2011)
CCSM4	National Center for Atmospheric Research, USA	1.25° × 0.94°	(Gent et al., 2011)
CNRM-CM5	*Centre National de Recherches Météorologiques* and *Centre Européen de Recherche et de Formation Avancées en Calcul Scientifique*, France	1.4° × 1.4°	(Voldoire et al., 2013)
GFDL-CM3	NOAA Geophysical Fluid Dynamics Laboratory, USA	2.5° × 2.0°	(Donner et al., 2011)
GFDL-ESM2G		2.5° × 2.0°	(Dunne et al., 2012)
GFDL-ESM2M		2.5° × 2.0°	(Dunne et al., 2012)
HadGEM2-ES	Met Office Hadley Centre, UK	1.875° × 1.25°	(Bellouin et al., 2011)
INM-CM4	Institute for Numerical Mathematics, Russia	2.0° × 1.5°	(Volodin et al., 2010)
IPSL-CM5A-LR	*Institut Pierre-Simon Laplace*, France	3.75° × 1.875°	(Dufresne et al., 2013)
IPSL-CM5A-MR		2.5° × 1.25°	(Dufresne et al., 2013)
MIROC5	Atmosphere and Ocean Research Institute (The University of Tokyo), National Institute for Environmental Studies, and Japan Agency for Marine-Earth Science and Technology	1.4° × 1.4°	(Watanabe et al., 2010)
MIROC-ESM-CHEM		2.8° × 2.8°	(Watanabe et al., 2011)
MIROC-ESM		2.8° × 2.8°	(Watanabe et al., 2011)
MRI-CGCM3	Meteorological Research Institute/ Japan Meteorological Agency	1.1° × 1.1°	(Yukimoto et al., 2012)
NorESM1-M	Norwegian Climate Centre	2.5° × 1.875°	(Bentsen et al., 2013)

spatial–temporal scale to the HUC8, monthly scale.

2.4. Future projections of potential vegetation with the MC2 DGVM and integration with WaSSI

The MC2 DGVM can project future changes in vegetation type and state (e.g., LAI, biomass) in response to climate change and increasing atmospheric CO_2. The MC2 DGVM is a refactored version of the MC1 DGVM (Bachelet et al., 2001; Conklin et al., 2016), with no change in science but with improvements in computational performance (Kim et al., 2018). MC2 consists of 3 submodels that address biogeochemistry (CENTURY Soil Organic Matter Model; Parton et al., 1993), fire disturbance (MC-Fire fire simulation model; Conklin et al., 2016), and biogeography (MAPSS vegetation biogeography model; Neilson, 1995). A full technical description of MC2 is available in Bachelet et al. (2001) and Conklin et al. (2016).

For integration with WaSSI (Fig. 2), we obtained future projections of potential natural vegetation from MC2 simulations under the same scenarios and climate forcing described in Section 2.3 (EPA, 2017). Annual outputs of vegetation type and LAI at the 1/16° spatial scale were adapted as input into WaSSI. First, we translated the ~50 vegetation types output by MC2 into one of the six natural vegetation types defined by WaSSI (i.e., deciduous, evergreen, and mixed forests; shrubland, grassland, and barren land), and then applied a natural vegetation mask based on the 2006 NLCD product (USGS, 2011) to all MC2 grid cells, masking out the areas characterized by other land cover types (e.g., urban areas, croplands, and artificial pasture). Second, we aggregated the MC2 results per ecoregion (level-2 ecoregions of North America; EPA, 2010; Fig. 3), obtaining the area fraction for each vegetation type, related to the total natural vegetation area, and the respective LAI. HUC8 polygons have fine spatial resolution in relation to the 1/16° grid resolution used by MC2, with some HUC8 polygons coinciding with as few as a single 1/16° grid cell. We extracted a regional signal from MC2 output to increase our confidence in its vegetation projections. Third, from the ecoregion-level results, we calculated the anomalies in vegetation area fraction and LAI for years 2007–2099 relative to a 2000–2006 mean baseline. Finally, we combined the default vegetation boundary conditions in WaSSI, based on 2006 NLCD and 2000–2006 mean monthly MODIS LAI, with the anomalies derived from the MC2 simulations to create, for each natural vegetation type, a time series of annual area fraction and monthly LAI for 2007–2099 at the HUC8 scale. We only let the natural vegetation fraction of each HUC8 to be dynamic. The remaining land cover types considered in WaSSI (urban, cropland, wetland, and water) were kept constant over time. A more detailed description of our procedure to create the dynamic vegetation boundary conditions within WaSSI is given in Appendix A.

2.5. Simulation experiments and data analysis

To assess the combined impact of climate and vegetation change on water yield, we carried out an ensemble of 16 simulations with the revised WaSSI model (Section 2.2) for each RCP scenario (4.5 and 8.5, totaling 32 simulations), using LOCA-downscaled climate projections from 16 GCMs (Section 2.3) and the corresponding MC2-based vegetation projections (Section 2.4), covering years 2007 to 2099. To assess the individual impacts of direct climate change (i.e., changes in air temperature and precipitation) and climate-induced vegetation change on water yield, we ran two additional WaSSI simulation ensembles: the first with dynamic climate and *fixed vegetation* (i.e., annual area fraction and monthly LAI of each vegetation type fixed at their year 2007 values, looped throughout the simulation), and the second with *fixed climate* (i.e., monthly temperature and precipitation values for year 2007, looped throughout the simulation) and dynamic vegetation, all else was the same as in main simulation ensemble.

We calculated future changes in water yield and in other relevant model outputs (e.g., ET, soil moisture) and inputs (e.g., air temperature, precipitation, vegetation cover fraction, LAI) for mid-century (2040–2059) and end-century (2080–2099) relative to a "present-day" (2008–2027) baseline. We disregarded the first simulation year (2007) as it was used for WaSSI spin-up. We calculated mean ensemble differences between climatological periods (i.e., mid-century – present, end-century – present) for RCP 4.5 and 8.5, and determined their statistical significance via Student's *t* test (dependent *t* test for paired samples). The calculations were done at the HUC8 and HUC2 scales (Fig. 1).

We also investigated hydrological changes at the regional level by using the Budyko framework (Budyko, 1958). We averaged ET, PET, and precipitation at the HUC2 scale for each climatological period, and then calculated an evaporative index (ET/P) and an aridity index (PET/P). We then ensemble averaged the indices for each climatological period under RCP 4.5 and 8.5. The statistical significance of the differences between climatological periods was determined via Student's *t* test (dependent *t* test for paired samples). For each period and RCP scenario, we adjusted an overall Budyko curve in $ET/P \times PET/P$ space for CONUS based on results for all 18 HUC2s (Fig. 1). We chose the Fu (1981) model:

$$\frac{ET}{P} = 1 + \left(\frac{PET}{P}\right) - \left(1 + \left(\frac{PET}{P}\right)^{\omega}\right)^{\frac{1}{\omega}} \quad (3)$$

where ω is an empirical parameter (adjustable) representing overall

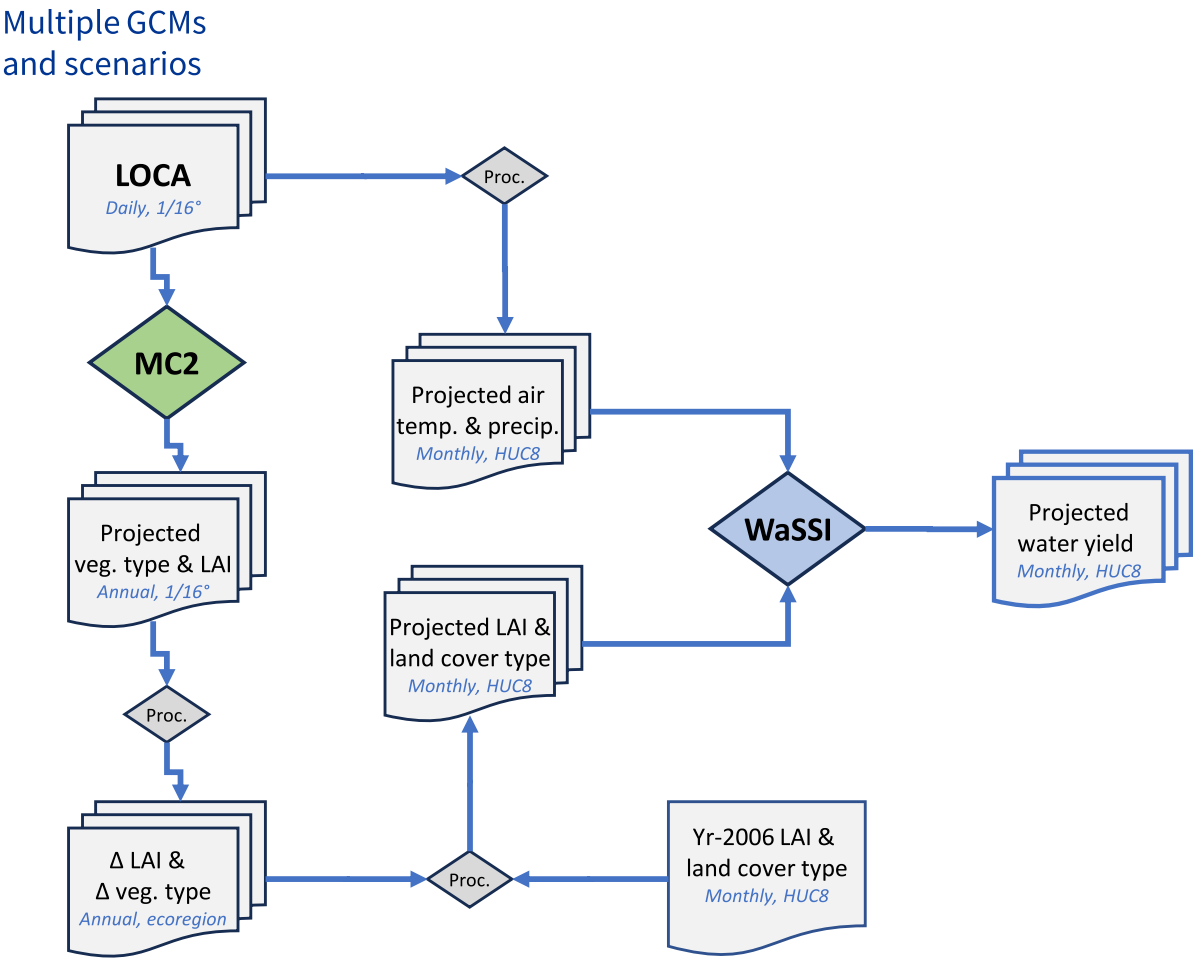

Fig. 2. WaSSI-MC2 integration overview. High resolution (daily, 1/16°) future climate projections with multiple GCMs and scenarios (LOCA; Pierce et al., 2015, 2014) are used to drive the MC2 DGVM. The projected potential natural vegetation types and LAI (MC2 DGVM annual outputs) are first translated to WaSSI natural vegetation classes and integrated at the ecoregion level (Fig. 3). Then, anomalies are calculated relative to a 2000–2006 baseline. The natural vegetation type and LAI anomalies at the ecoregion level are combined with land cover "observations" for year ~2006 at the monthly, HUC8 scale (based on 2006 NLCD and 2000–2006 MODIS data products, as originally defined in WaSSI) to project future land cover (2007–2099), which is then used as input in WaSSI. Note that only changes in natural vegetation are projected, while the other land cover classes in WaSSI are kept fixed on year ~2006 values. The climatic driver for WaSSI is created by integrating precipitation and air temperature from the LOCA downscaled climate projections at the monthly, HUC8 scale. With the dynamic climate and land cover inputs, WaSSI is run to project future hydrology. In the flow chart, "Proc." (gray diamonds) indicates data processing steps. See Section 2.4 for further details.

catchment properties.

2.6. Validation of the 2008–2027 "Present-Day" baseline

For validation purposes, we compared mean annual LOCA-downscaled projections of surface air temperature and precipitation for the 2008–2027 "present-day" baseline at the HUC8 level in CONUS against 2008–2023 mean annual observations from PRISM (PRISM Climate Group, 2024). We also compared 2008–2027 mean annual ET simulated with WaSSI against 2008–2023 mean annual MODIS ET (Running et al., 2021). Monthly PRISM and annual MODIS ET data were aggregated at the HUC8 level from original spatial resolutions of 4 km and 500 m, respectively.

3. Results

3.1. Accuracy of the 2008–2027 "Present-Day" baseline

Mean annual air temperature and precipitation projected for 2008–2027 under RCP 8.5 for the HUC8s in CONUS (LOCA dataset) are tightly correlated (r = 0.99) with mean annual PRISM observations for 2008–2023 (Fig. 4a,b), with small mean bias errors (MBE) of 0.48 °C and − 37 mm yr^{-1} and root mean square errors (RMSE) of 0.82 °C and 83 mm yr^{-1}. Mean annual ET projected for 2008–2027 under RCP 8.5 based on WaSSI is highly correlated (r = 0.86) with mean annual MODIS ET for 2008–2023 (Fig. 4c), with a reasonably small MBE of 25 mm yr^{-1} and RMSE of 118 mm yr^{-1}. In each comparison (*T*, *P*, ET), the linear regression exhibits a slope close to 1 and an intercept close to 0 (see Fig. 4). Results under RCP 4.5 are virtually identical to those presented here (not shown). This demonstrates that our "present-day" simulations can be used as the baseline for the calculation of the relative changes for mid-century and end-century.

3.2. Change in climate and land cover

Air temperature is projected to significantly increase across CONUS at mid-century and end-century under scenarios RCP 4.5 and RCP 8.5, based on the LOCA climate projections (Fig. 5a,b, S1a,b). Under RCP 4.5, the changes at the HUC2 scale relative to "present day" vary from 0.98 to 1.43 °C (mid-century) and 1.62 to 2.41 °C (end-century), while under RCP 8.5, the changes are roughly twice as high: 1.47 to 2.09 °C (mid-century) and 3.72 to 5.28 °C (end-century).

The projected precipitation changes across CONUS based on LOCA are less clear compared to the projected air temperature changes,

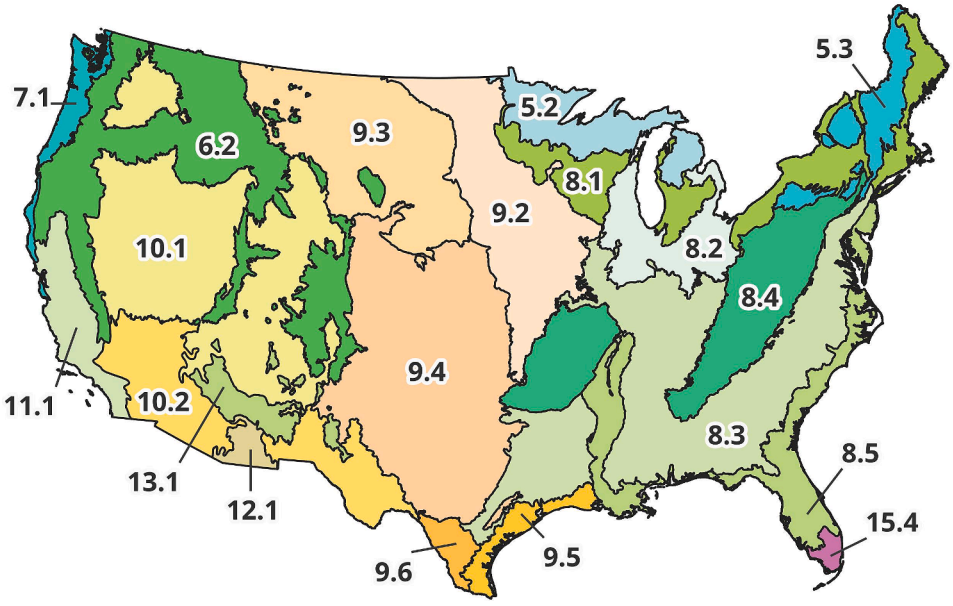

Fig. 3. Level-2 ecoregions in CONUS (EPA, 2010): 5.2 Mixed wood shield, 5.3 Atlantic highlands, 6.2 Western cordillera, 7.1 Marine west coast forest, 8.1 Mixed wood plains, 8.2 Central USA plains, 8.3 Southeastern USA plains, 8.4 Ozark/Ouachita-Appalachian forests, 8.5 Mississippi alluvial and southeast USA coastal plains, 9.2 Temperate prairies, 9.3 West-central semiarid prairies, 9.4 South central semiarid prairies, 9.5 Texas-Louisiana coastal plain, 9.6 Tamaulipas-Texas semiarid plain, 10.1 Cold deserts, 10.2 Warm deserts, 11.1 Mediterranean California, 12.1 Western Sierra Madre piedmont, 13.1 Upper Gila mountains, 15.4 Everglades.

especially due to the high variability across GCMs (Fig. 5c,d, S1c,d). For most regions, the projected precipitation changes at mid- and end-century under scenarios RCP 4.5 and 8.5 are statistically insignificant. The projected precipitation changes at end-century under scenario RCP 8.5 exhibit a relatively clearer pattern, with statistically significant increases (decreases) in the order of 10% at many northern (southern) HUC8s (Fig. 5d).

Based on MC2 simulations of potential natural vegetation and "present-day" observations, our projected changes in vegetation type and LAI show similar spatial patterns under RCP 4.5 and 8.5, with more pronounced changes under the latter scenario (Figs. 6 and 7; see also Figs. S2 and S3). At end-century and under RCP 8.5, notable vegetation type shifts include: 1) mixed forest to deciduous forest in the northern Appalachians and upper Midwest; 2) deciduous forest to mixed/evergreen forest in the southern Appalachians; 3) evergreen forest to mixed forest in the Pacific Northwest; 4) grassland to shrubland in the Intermountain West; and 5) shrubland to grassland in the Great Plains, with changes of up to ≈ 0.28, 0.11, 0.46, 0.10, and 0.06 in HUC8 coverage area fraction, respectively (Fig. 7). Also notable is the projected increase in evergreen forest coverage in the southeastern coastal plains and western mountain ranges (i.e., up to ≈ 0.08 in HUC8 coverage area fraction), associated with a combined coverage reduction of other vegetation types. For the same period and scenario, total LAI is projected to increase in the western mountain ranges, southern Great Plains, and southeastern coastal plains, and decrease in parts of the Intermountain West and Appalachians, with relative changes reaching up to $\approx +33\%$, $+10\%$, $+14\%$, -10%, and -5% at the HUC8 scale, respectively (Fig. 7g). Under RCP 4.5, the projected shift in vegetation type in the northern Appalachians and Pacific Northwest at end-century also stands out, but is less pronounced than under RCP 8.5 (changes in HUC8 coverage area fraction of up to ≈ 0.22 (mixed forest to deciduous forest) and ≈ 0.20 (evergreen forest to mixed forest), respectively; see Fig. 6). In other regions, the projected shift in vegetation type is generally similar as under RCP 8.5, but displaying lower magnitudes and oftentimes a lack of statistical significance. The same applies to the projected changes in LAI. In the western mountains and southeastern coastal plains, the projections indicate an increase of up to about 15% and 8% at the HUC8 scale, respectively, and a decrease of up to about 9% in the Intermountain West (Fig. 6g).

At mid-century, under both RCP 4.5 and 8.5 scenarios, the projected changes in vegetation type and LAI across CONUS are generally statistically insignificant (Figs. S2 and S3). Notable exceptions are the northern Appalachians and the Pacific Northwest, which present statistically significant changes in vegetation type in the same direction as described above.

3.3. Change in evapotranspiration

Based on our WaSSI simulations, ET is projected to significantly increase across CONUS under RCP 4.5 and 8.5 at mid-century (Fig. S4a,b) and end-century (Fig. 8a,b), except generally for portions of the Southwest and Great Plains, in which the projected changes are statistically insignificant. The projected increase in ET is notably stronger in the North, Northeast, and Rocky Mountains. ET is projected to significantly increase in 12 HUC2s at mid-century and end-century under both RCP 4.5 and 8.5, ranging from 2% to 6% (3% to 7%) at mid-century and 4% to 9% (8% to 20%) at end-century under RCP 4.5(8.5) (Fig. 9). Conversely, the projected changes for HUCs 12-Texas-Gulf, 13-Rio Grande, 15-Lower Colorado, and 18-California for both periods and scenarios are statistically insignificant. In HUCs 11-Arkansas-White-Red and 16-Great Basin, ET is projected to significantly increase at end-century under both scenarios.

3.4. Change in water yield

Water yield is projected to significantly decrease across vast areas of CONUS, especially at end-century under RCP 8.5 (Fig. 8c,d and S4c,d). Virtually no significant increase is projected. Under RCP 8.5, a substantial decrease in water yield is projected for HUC8s in the central and southeastern U.S. (up to $-47(-75)\%$ and -102 (-207) mm year^{-1} at mid-century (end-century)), while statistically insignificant changes are projected for the western and northeastern U.S. Under RCP 4.5, the projected changes in water yield are substantially smaller, lacking statistical significance for most of CONUS, except generally for areas in the central and southeastern U.S., with HUC8 changes of up to $-38(-40)$ % and $-74(-71)$ mm year^{-1} at mid-century (end-century). Water yield is

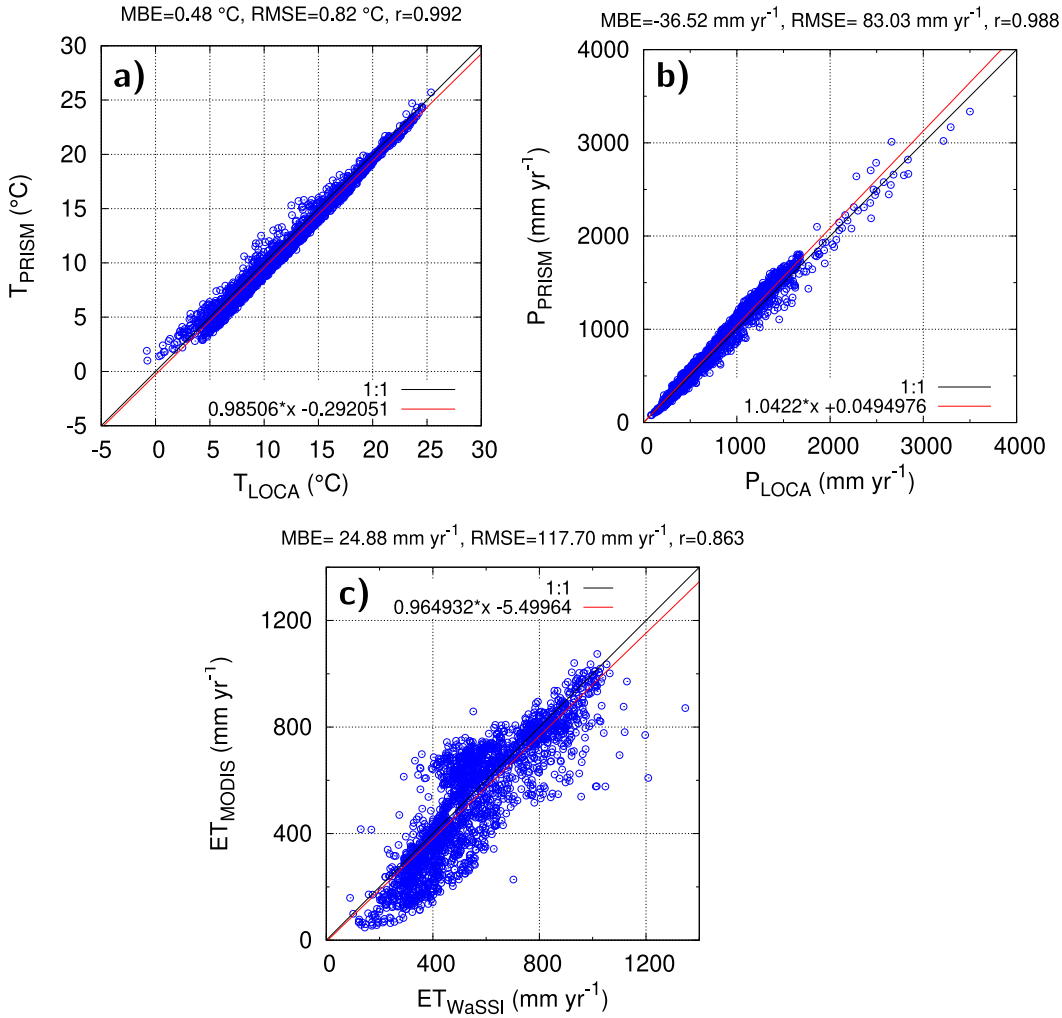

Fig. 4. Comparison of mean annual "present-day" (2008–2027) projections under RCP 8.5 against mean annual observations (2008–2023) for each HUC8 in CONUS (n = 2099): a) surface air temperature (LOCA projection vs. PRISM data), b) precipitation (LOCA projection vs. PRISM data), and c) evapotranspiration (WaSSI projection vs. MODIS data). Projections correspond to ensemble averages (16 GCMs; see Table 1).

projected to significantly decrease in four HUC2s at mid-century and end-century under both RCP 4.5 and 8.5 (8-Lower Mississippi, 10-Missouri, 11-Arkansas-White-Red, and 13-Rio Grande), ranging from −14 (−18) % to −8(−10) % and −41(−55) mm year^{-1} to −3(−4) mm year^{-1} at mid-century and −14(−30) % to −7(−22) % and −41 (−122) mm year^{-1} to −3(−7) mm year^{-1} at end-century under RCP 4.5 (8.5) (Fig. 10). Conversely, the projected changes for HUCs 1-New England, 16-Great Basin, 17-Pacific Northwest, and 18-California for both periods and scenarios are statistically insignificant. In HUCs 7-Upper Mississippi and 9-Souris-Red-Rainy, water yield is projected to significantly decrease at end-century under both scenarios.

3.5. Change in soil moisture

Soil moisture is projected to significantly decrease across most of CONUS at mid-century (Fig. S4e,f) and end-century (Fig. 8e,f) under both RCP 4.5 and 8.5 (in our paper, unless otherwise specified, "soil moisture" refers to total column soil moisture). Virtually no significant increase is projected. At end-century under RCP 8.5, soil moisture is projected to significantly decrease across virtually all HUC8s. The projected changes are substantial in the central and western US, reaching up to −28(−49) % and −0.14(−0.27) at the HUC8 scale at mid-century (end-century) under RCP 8.5, and −24(−30) % and −0.10(−0.13) under RCP 4.5. Soil moisture is projected to significantly decrease in 14 HUC2s at mid-century and end-century under both RCP 4.5 and 8.5 (all HUC2s but 1-New England, 2-Mid-Atlantic, 4-Great Lakes, and 15-Lower Colorado), ranging from −12(−16) % to −1(−2) % and −0.05(−0.06) to −0.01(−0.02) at mid-century and −13(−31) % to −2(−5) % and −0.06(−0.13) to −0.01(−0.04) at end-century under RCP 4.5(8.5) (Fig. 11). In HUCs 4-Great Lakes and 15-Lower Colorado, soil moisture is projected to significantly decrease at end-century under both scenarios.

3.6. Change in aridity and evaporative indices

Our projections indicate a significant change in the Budyko space towards higher aridity and evaporative indices for virtually all HUC2s at mid- and end-century under RCP 4.5 and 8.5 (Fig. 12). Changes are more substantial at end-century and under RCP 8.5 (Fig. 12d). Overall, the "present-day" and projected future values (origin and tip of the vectors in Fig. 12, respectively) follow a Budyko curve. The adjusted ω parameter in Fu's equation (3) slightly drops from 2.59(2.58) to 2.55(2.52) at mid-century and to 2.52(2.43) at end-century under RCP 4.5(8.5). Interestingly, the HUC 18-California notably deviates from the Budyko curve for all periods and scenarios, with relatively small ET/P for the given PET/P value. In HUC 18-California, the projected changes in aridity index are statistically significant at mid- and end-century under both scenarios, but the changes in evaporative index are not (except for a small change at mid-century under RCP 4.5, Fig. 12a). The projected

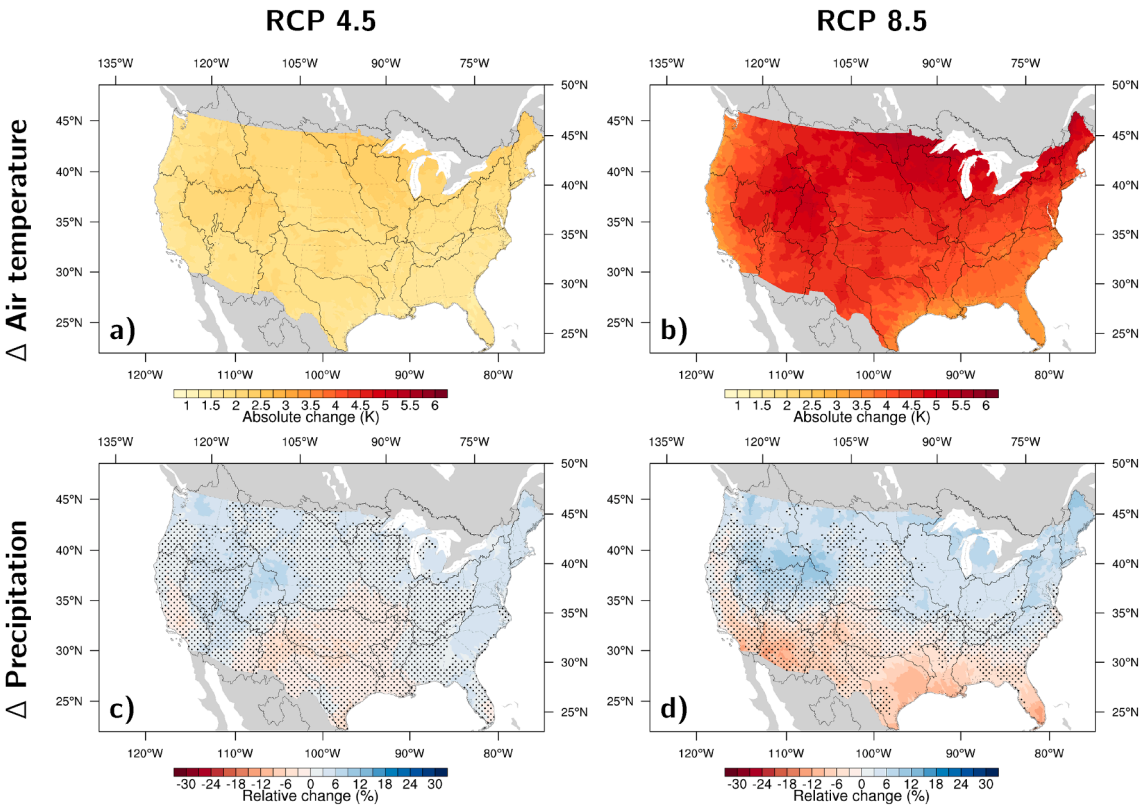

Fig. 5. Projected changes in air temperature (**a**, **b**) and precipitation (**c**, **d**) at end-century (2080–2099) under scenarios RCP 4.5 and 8.5, respectively, at the HUC8 scale, based on the LOCA downscaled climate dataset. Absolute changes in air temperature and percent changes in precipitation relative to "present day" (2008–2027) are shown. The hatched pattern indicates insignificant changes at the 95 % confidence level. HUC2s are delineated in black.

changes in evaporative index for HUCs 16-Great Basin and 15-Lower Colorado at mid/end-century under RCP 4.5 are also insignificant, while the projected changes in aridity index are significant (except for HUC 15-Lower Colorado at mid-century; in this case the projected changes in both indices are insignificant; Fig. 12a,c).

3.7. Drivers of water yield change

Our "fixed-vegetation" and "fixed-climate" sensitivity simulations indicate a much stronger impact (i.e., 1 order of magnitude higher) of direct climate change (i.e., changes in precipitation and air temperature) on future water yield, compared to the impact of vegetation change (Figs. 13 and S5). The projected end-century changes in water yield under RCP 8.5 with the "fixed-vegetation" simulation (Fig. 13c,d), highlighting the impact of climate change on water yield, differs little from our standard simulation with dynamic climate and dynamic vegetation (Fig. 13a,b; see also Fig. 13g,h). In the former case, significant changes vary from −75 to 47% and −207 to 153 mm year^{-1} at the HUC8 scale, while in the latter, changes vary from −75 to 47% and −207 to 139 mm year^{-1}. The projected changes with the "fixed-climate" simulation (Fig. 13e,f), highlighting the impact of vegetation change on water yield, are generally significant in forest areas of the Northeast, Southeast, and western mountains. The significant changes vary from −7 to 8% and −23 to 14 mm year^{-1} at the HUC8 scale, with typically positive values in the Northeast, negative values in the Southeast, and mixed values in the western mountains. Note that the projected changes in water yield (Fig. 13e,f) are inversely correlated with the projected changes in LAI (Fig. 7g). The magnitude of the ratio between significant "fixed-climate" and "fixed-vegetation" absolute changes in water yield (vegetation and climate change impacts on water yield, respectively) varies from 0.02 to 47% at the HUC8 scale, with first, second, and third quartiles of 1, 3, and 9%, respectively. Under RCP 4.5, the impact of climate change on water yield is smaller than under RCP 8.5 (Fig. S5c,d), but so is the impact of vegetation change (Fig. S5e,f), resulting in similar vegetation/climate change impact ratios.

4. Discussion

4.1. Overall Spatial-Temporal patterns of change

4.1.1. Land cover

Our projected changes in land cover (Figs. 6 and 7), based on available MC2 simulations, reflect projected changes in climate and wildfire occurrence and effects. Overall, our projected changes in vegetation type are consistent with latitudinal and elevational shifts in vegetation distribution under a warmer climate, as shown in previous studies (e.g., Gonzalez et al., 2010; Grimm et al., 2013). Our projected changes in LAI are generally comparable with other simulations, but more shifted towards negative values (i.e., decreases). Mahowald et al. (2016) assessed global LAI projections from 18 CMIP5 GCMs, 11 of which has dynamic vegetation simulation capability. Their projections generally show larger LAI values across CONUS at end-century under RCP 8.5 (2081–2100 vs. 1981–2000), with absolute changes ranging from about −0.15 to 1.05 m^2 m^{-2} when all 18 GCMs were considered and from 0.15 to 0.75 m^2 m^{-2} when only the top 50% performing GCMs were considered (based on historical observations of LAI) (Mahowald et al., 2016). For comparison, we found in our study that, under RCP 8.5, the end-century absolute changes can reach up to about 0.35 m^2 m^{-2} in the Southeast and Northwest, −0.10 m^2 m^{-2} in the Appalachians, 0.10 m^2 m^{-2} in the Rockies, and ± 0.04 m^2 m^{-2} in the central U.S. (percent changes shown in Fig. 7). We used a different baseline period (i.e., 2008–2027), which could partially explain the smaller changes in our study. Also, the simulations analyzed by Mahowald et al. (2016) correspond to fully-coupled global runs at coarse spatial scales of about

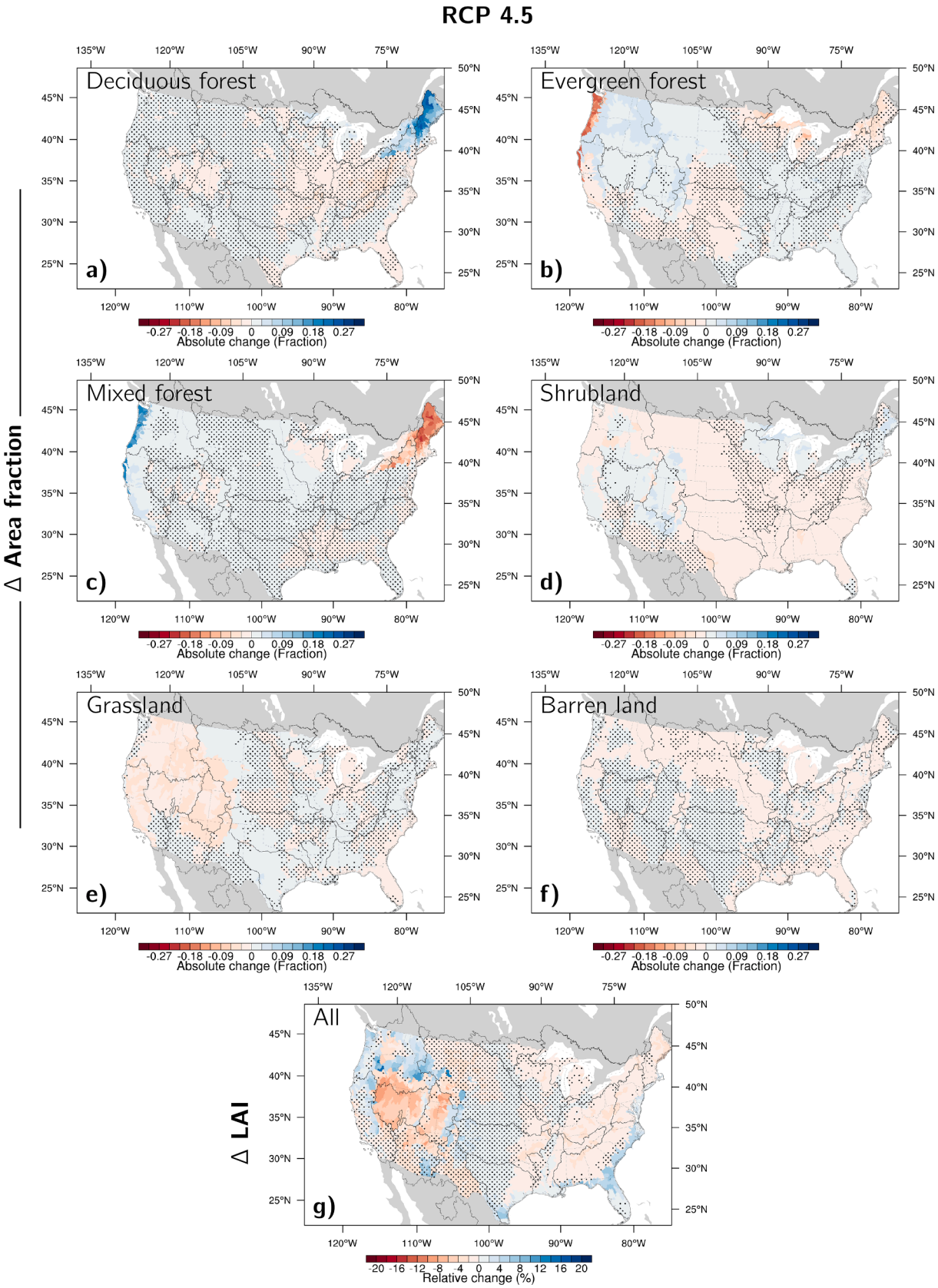

Fig. 6. Projected changes in vegetation type and LAI at end-century (2080–2099) under scenario RCP 4.5 at the HUC8 scale, based on MC2 projections and "present-day" observations. Absolute changes in coverage area fraction are shown for deciduous forest (**a**), evergreen forest (**b**), mixed forest (**c**), shrubland (**d**), grassland (**e**), and barren land (**f**), relative to "present day" (2008–2027). Percent changes in total LAI relative to 2008-2027 are shown in panel **g**. The hatched pattern indicates insignificant changes at the 95% confidence level. HUC2s are delineated in black.

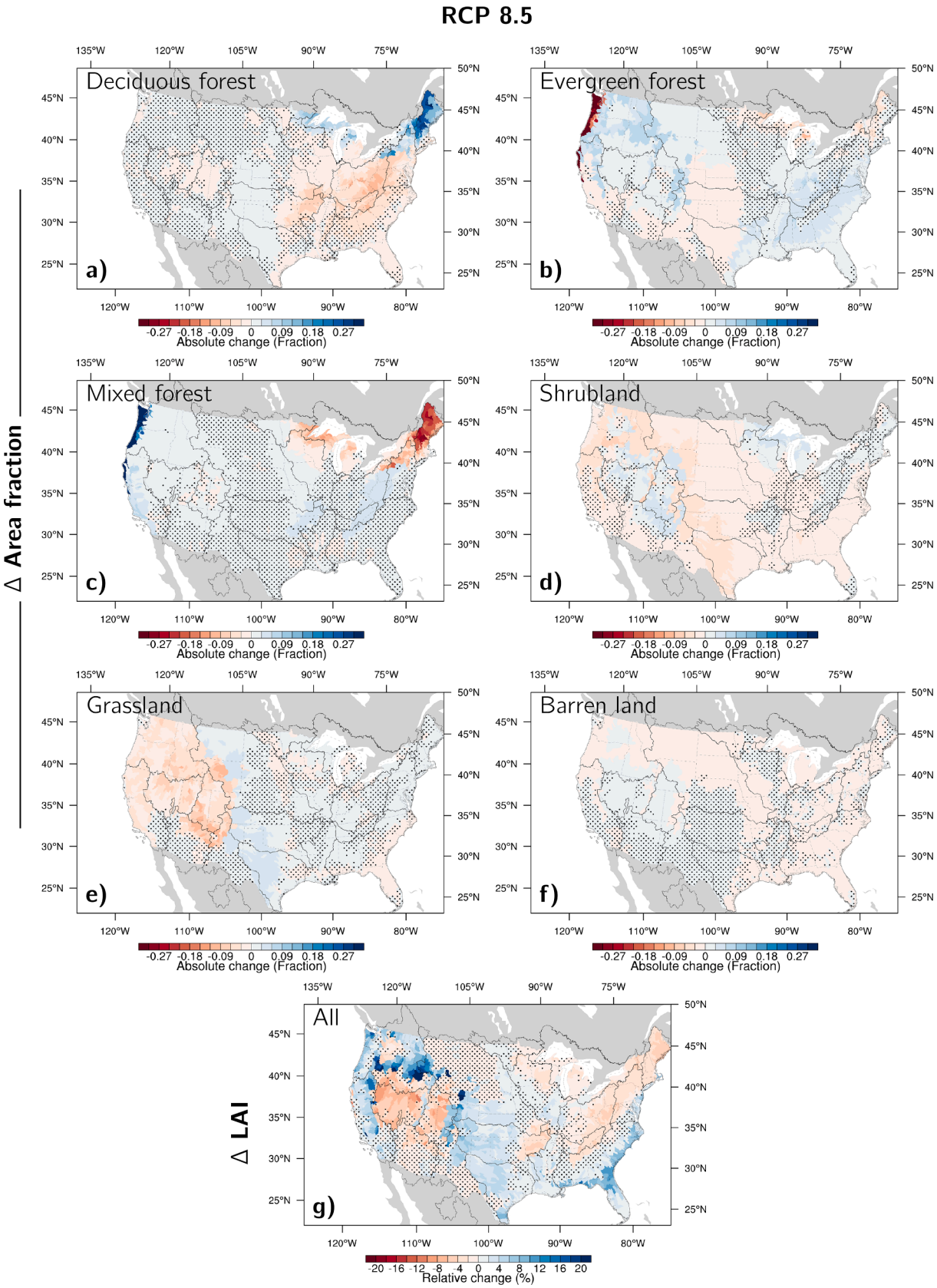

Fig. 7. Same as Fig. 6, but for scenario RCP 8.5.

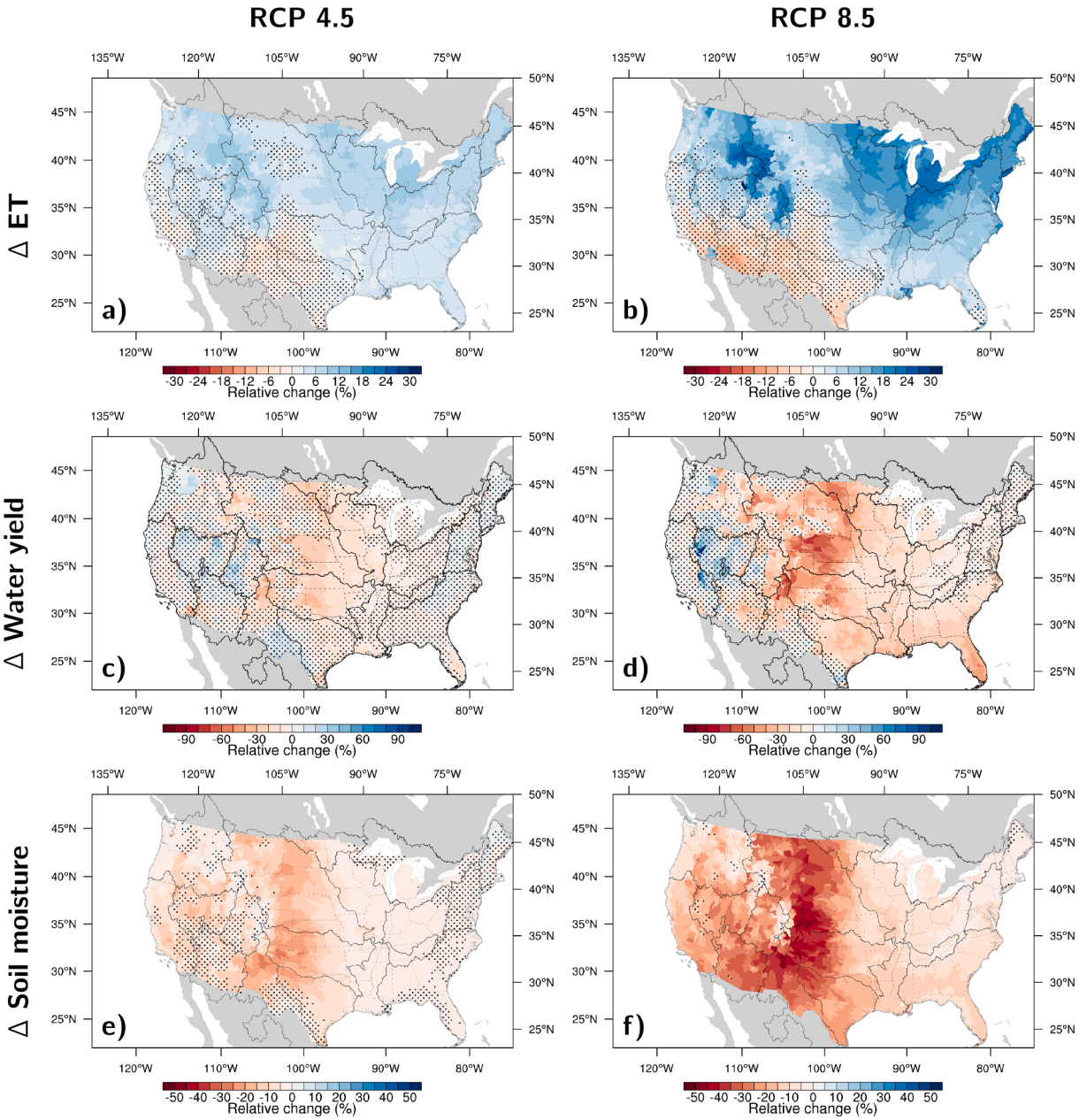

Fig. 8. Projected changes in ET (**a**, **b**), water yield (**c**, **d**), and soil moisture (**e**, **f**) at end-century (2080–2099) under scenarios RCP 4.5 and 8.5, respectively, at the HUC8 scale, based on WaSSI output. Percent changes relative to "present day" (2008–2027) are shown. The hatched pattern indicates insignificant changes at the 95% confidence level. HUC2s are delineated in black.

2°. We also compared, at the ecoregion level in CONUS, the original MC2 LAI projections that we started with against available DGVM LAI projections from the Inter-Sectoral Impact Model Intercomparison Project (ISIMIP; Reyer et al., 2019). We examined global simulations from five different DGVMs at ½° spatial resolution, each one driven by climate projections from 1 to 4 CMIP5 GCMs under RCP 6.0, assuming no land use change in the future (ISIMIP Protocol 2b, Experiment III; simulations under RCP 8.5 climate and CO_2 were unavailable except for one DGVM, so we used the closest scenario, RCP 6.0). We found that the future LAI anomalies projected with MC2 under RCP 8.5 were comparable with the ISIMIP projections. However, the ISIMIP results generally indicate positive LAI trends, while the MC2 results indicate approximately neutral or negative trends for most ecoregions (not shown). Different RCP scenarios, selection of GCMs, spatial resolution (1/16° in MC2 vs. ½° in ISIMIP) and GCM climate downscaling could partially explain the differences in projected LAI.

4.1.2. *Evapotranspiration*

Our projections indicate a substantial increase in ET across much of CONUS, except generally for water-limited areas in the South and Southwest (Figs. 8, 9, S4). The spatial patterns of change are generally similar to those projected by Mahat et al. (2017) (2071–2090 vs. 1991–2010, RCP 4.5, 8.5) based on VIC simulations with statistically downscaled climate outputs from 7 CMIP5 GCMs (BCCA product). It is important to note that our results reflect the modeling approach for PET within WaSSI. Here we used the default configuration in WaSSI, in which PET is calculated based on near-surface air temperature and the daytime length defined by latitude and day of the year (Hamon, 1963). Duan et al. (2017) compared PET projections for CONUS with Hamon's formulation and an implementation of Penman-Monteith's formulation for a reference crop surface (Allen et al., 1998), and found substantially larger PET values with the former towards the end of the century, noting that Hamon's PET does not account for the attenuation expected with

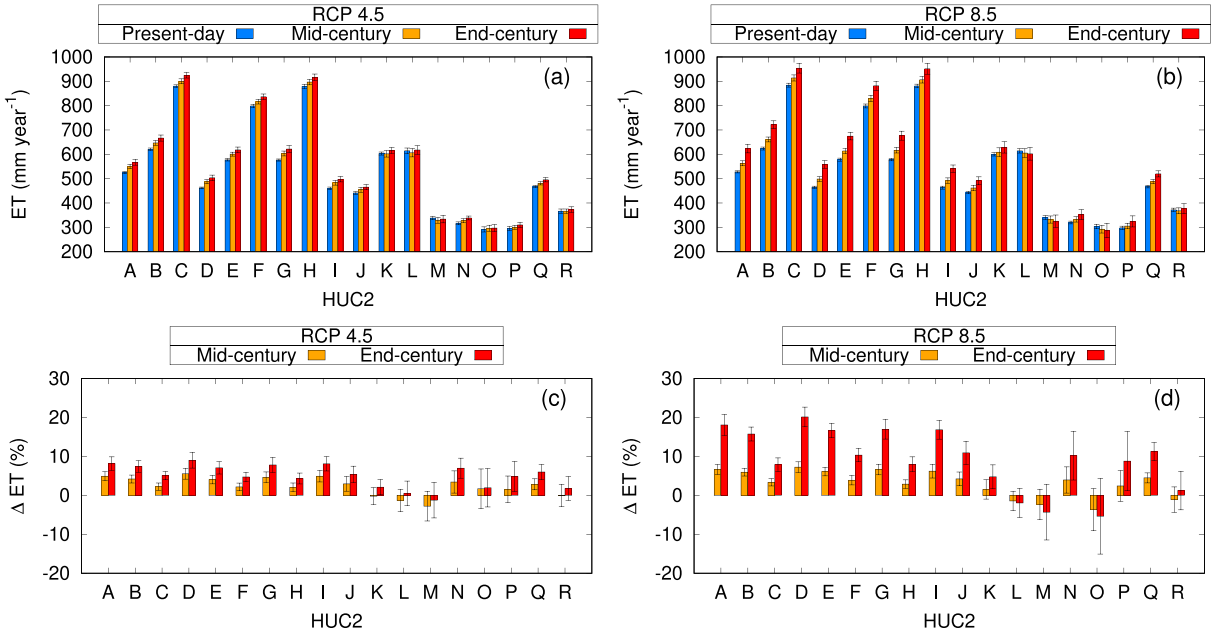

Fig. 9. Projected changes in ET at the HUC2 scale, based on WaSSI output (see corresponding HUC2 map in Fig. 1). Average "present-day" (2008–2027), mid-century (2040–2059), and end-century (2080–2099) values under scenarios RCP 4.5 and 8.5 are shown in panels a and b, respectively. The percent differences at mid-century and end-century relative to "present day" are shown in panels c and d for scenarios RCP 4.5 and 8.5, respectively. Error bars indicate a 95% confidence interval.

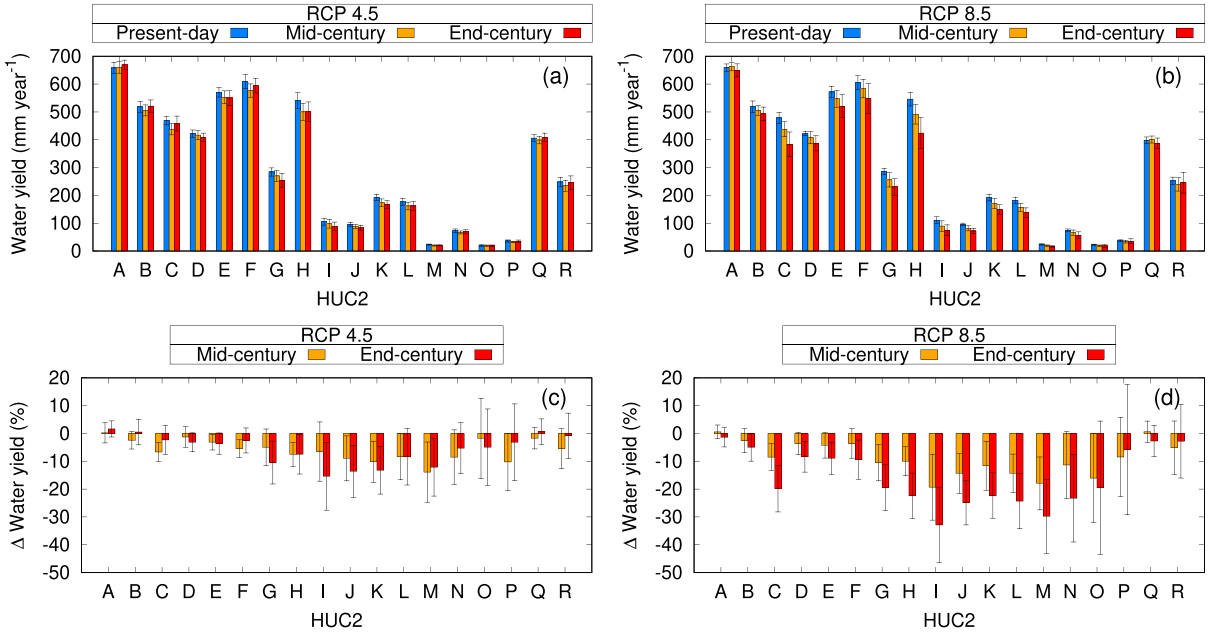

Fig. 10. Same as Fig. 9, but for water yield.

the projected increase in specific air humidity. The Penman-Monteith reference crop ET takes into consideration air temperature, specific air humidity, wind speed, and net radiation, being widely used and regarded as a reliable approach to estimate PET. At the same time, the downside of Penman-Monteith-based formulations is the dependence on additional meteorological variables, which may be unavailable or highly uncertain in future climate projections from GCMs. Here we opted for the default configuration (Hamon's PET) in WaSSI given its simplicity. Note that we used the LOCA downscaled climate projections to drive WaSSI, for consistency with the adopted MC2 vegetation projections, and that LOCA does not provide all meteorological variables necessary to calculate PET via a Penman-Monteith-based approach.

4.1.3. *Water yield*

Our projected changes in water yield across CONUS generally follow a similar spatial pattern to those of recent studies with the WaSSI and VIC models (Duan et al., 2017; Heidari et al., 2021a; Mahat et al., 2017). Our projections are remarkably similar to those in Duan et al., (2017; cf. their Fig. 5 and our Fig. 8). Note that they also used WaSSI and a large GCM ensemble (i.e., 20 GCMs, including 14 out of the 16 GCMs that we considered in our analysis). They also used scenarios RCP 4.5 and 8.5 and defined similar baseline, mid-century, and end-century periods for calculating the changes in water yield. Their simulations mainly differ from ours in terms of the downscaled climate dataset used (MACA vs. LOCA) and land cover boundary conditions (fixed vs. dynamic land

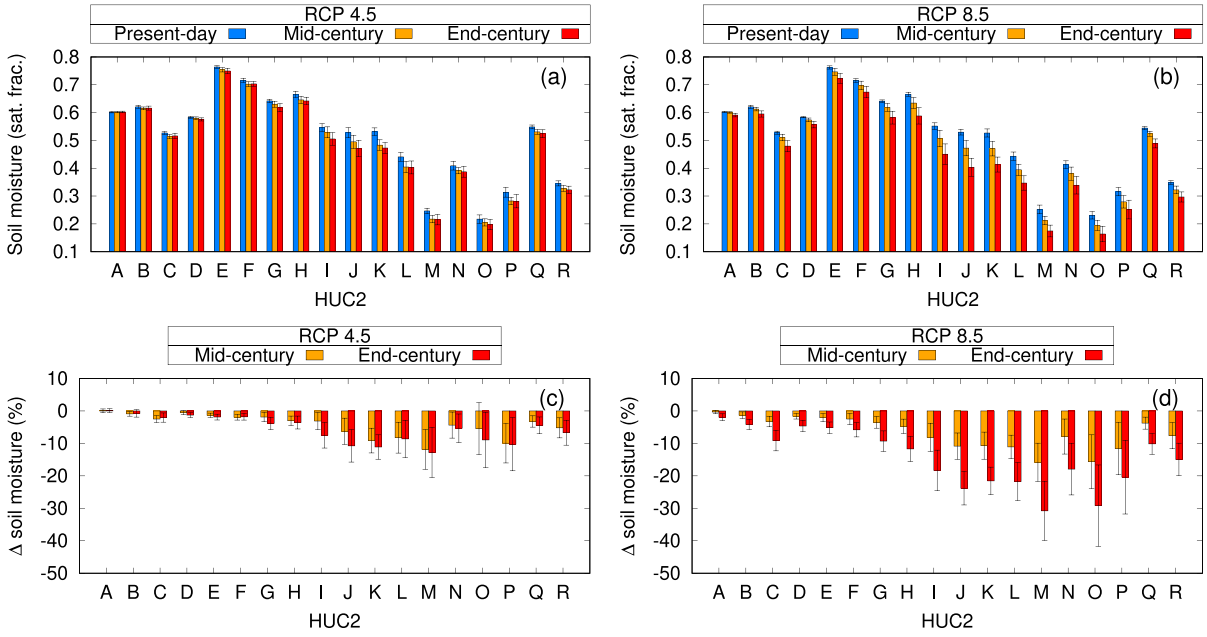

Fig. 11. Same as Fig. 9, but for soil moisture.

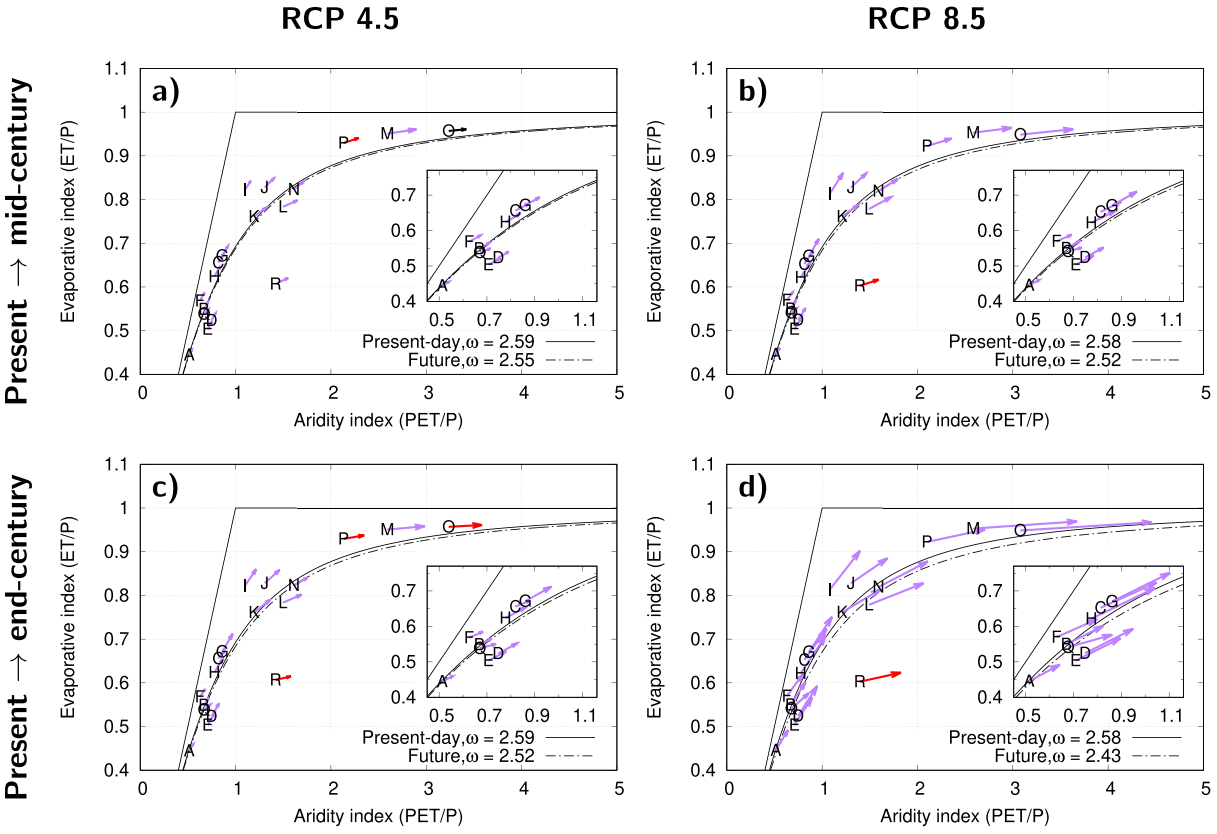

Fig. 12. Budyko diagrams based on projections of aridity and evaporative indices at the HUC2 scale with WaSSI (see corresponding HUC2 map in Fig. 1). Panels a and b show the projected mid-century (2040–2059) changes relative to "present day" (2008–2027) under scenarios RCP 4.5 and 8.5, respectively. Panels c and d show the projected end-century (2080–2099) changes relative to "present day" (2008–2027) under scenarios RCP 4.5 and 8.5, respectively. Purple vectors indicate significant changes at the 95 % confidence level in both *x* and *y* dimensions. Red vectors indicate significant changes only in the *x* dimension (aridity index). Black vectors indicate insignificant changes in both dimensions. The curves correspond to Fu's equation (3) (Fu, 1981), where ω is a fitting parameter. (For interpretation of the references to colour in this figure legend, the reader is referred to the web version of this article.)

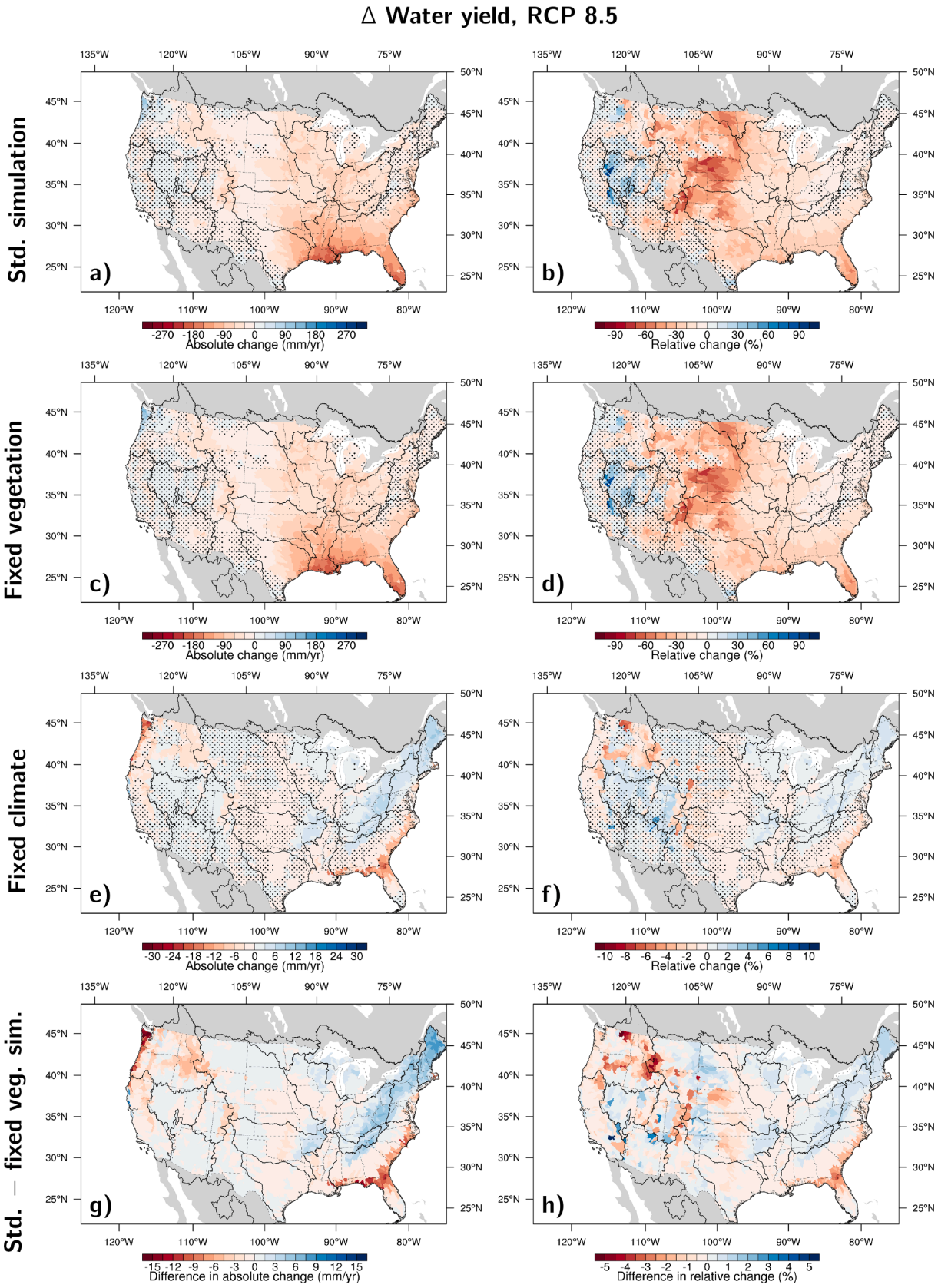

Fig. 13. Projected changes in water yield at end-century (2080–2099) under scenario RCP 8.5 relative to "present day" (2008–2027), based on WaSSI output. Results from three distinct simulations are shown, **a**,**b**) considering dynamic climate and dynamic vegetation (standard simulation), **c**,**d**) dynamic climate and fixed vegetation, and **e**,**f**) fixed climate and dynamic vegetation. Absolute (**a**,**c**,**e**) and percent (**b**,**d**,**f**) changes are shown at the HUC8 scale. The hatched pattern indicates insignificant changes at the 95% confidence level. HUC2s are delineated in black. Panels **g** and **h** show the difference between the results in **a** and **c** and **b** and **d**, respectively.

cover). Another important difference is that Duan et al. (2017) modified WaSSI to calculate PET as Penman-Monteith reference crop ET (Allen et al., 1998), while we used the default configuration in WaSSI (PET via Hamon, 1963). Compared to Duan et al., (2017; their Figs. 5 and 6), our projected decreases in water yield (central and southeastern U.S.) are generally more accentuated, while our projected increases (western and northeastern U.S.) are generally more attenuated and statistically insignificant. Such systematic differences between the two studies are consistent with the different approaches to PET. Duan et al. (2017) compared overall projected changes in water yield for CONUS with both PET methods, and found more negative projections when using the Hamon's method (≈ −8% vs. ≈−2% ensemble median for RCP 8.5/2080s – approximated from their Fig. 7). Additional differences between our projected water yield changes and those in Duan et al. (2017) could be related to the differences in GCM selection, GCM downscaling method, and approach to land cover change.

4.1.4. Soil moisture

Our projections of total column soil moisture indicate declines across much of CONUS (Figs. 8 and 11, S4), which is generally consistent with previous studies (e.g., Berg et al., 2017; Joo et al., 2020). For example, based on output from 25 CMIP5 GCMs under RCP 8.5, Berg et al. (2017) found a decrease in surface (0–10 cm) soil moisture across the entire CONUS, reaching about −14% in the Southwest at end-century (2070–2099 vs. 1976–2005; their Fig. 1a, top panel). When considering total column soil moisture, they still found a reduction across most of CONUS, especially in the Southwest and southern Great Plains, reaching up to about −12%, but also increases in portions of the Midwest and Rocky Mountains reaching up to about +6% (their Fig. 1a, mid panel). Based on output from ISIMIP (6 global impact models, each of which was driven with bias-corrected climate from 5 CMIP5 GCMs at ½° spatial resolution), Joo et al. (2020) projected changes in surface (0–50 cm) soil moisture of about −3% to −8% in the Southeast and −14% to −19% in the South at end-century under RCP 8.5 (2080–2099 vs. 1986–2005; their Fig. 1b). They also projected approximately neutral changes in the Midwest, northern Great Plains, and Northwest. In our study, we project changes in total column soil moisture reaching about −12% in the Southeast and −50% in the Great Plains, and more neutral changes in portions of the Northwest and Rocky Mountains (2080–2099 vs. 2008–2027, RCP 8.5; Fig. 8f). Different from Berg et al. (2017) and Joo et al. (2020), our projections indicate substantial declines in soil moisture in the northern Great Plains and stronger decreases in soil moisture overall. Differences could be partially explained by the differences in GCM selection and downscaling, model spatial resolution, and potential overestimation of ET in our simulations (PET via Hamon's formulation, Section 4.1.2).

4.1.5. Aridity and evaporative indices

The Budyko diagrams in Fig. 12 summarize our projected hydroclimatic changes at the regional (HUC2) and CONUS level. With few exceptions, our mid- and end-century projections under RCP 4.5 and 8.5 indicate consistent and significant changes towards higher aridity and increased ET (decreased water yield, Q) per unit precipitation ($Q/P = 1 - \mathrm{ET}/P$).

Equations linking the evaporative and aridity indices, including the often-used Fu's equation (3) (Fu, 1981), have been proposed in previous studies. In this equation, ω is an empirical parameter representing overall properties of the catchment (e.g., basin slope, basin area, land cover, vegetation cover, relative soil water storage, and relative infiltration capacity; Heidari et al., 2021b; Wang et al., 2021). In Fig. 12, we adjusted an overall ω for all HUC2s in CONUS for "present day", mid-century, and end-century under RCP 4.5 and 8.5. Except for HUC 18-California, the projections of evaporative and aridity indices for each HUC2 follow the general Budyko curve for each period and scenario (Fu's equation with the overall CONUS ω) reasonably closely.

California has a unique climate configuration in CONUS, spanning from hot desert climate in the South to tundra climate in the upper elevations of the Sierra Nevada, with most land characterized by a hot/warm-summer Mediterranean climate, with dry summers and wet winters (Beck et al., 2023). The negative deviation of HUC 18-California from the general Budyko curve (lower than "expected" ET/P) is likely associated with PET being off-phase with precipitation and a larger fraction of precipitation falling as snow, as discussed in Fang et al. (2016). With precipitation shifted away from high-PET summer months to low-PET winter months, the amount of precipitation that is partitioned to ET is expected to be lower compared to a more typical climate in which P and PET are in phase, resulting in lower ET/P for the same PET/P. Similarly, with more precipitation falling as snow, the amount of precipitation that is partitioned to ET is expected to be lower compared to a more typical climate with less snowfall and more rainfall, also resulting in lower ET/P for the same PET/P.

Our adjusted overall ω value for "present day" CONUS (2.58) is remarkably close to the overall value reported by Caracciolo et al. (2018), 2.63, based on historical (1948–2003) observations from 422 catchments across CONUS, spreading across five climatic zones. The deviation that we found for HUC 18-California is also consistent with their results, as they found a lower ω value (1.86) for the Mediterranean climate catchments (most of them in California). It is worth noting that ω is sensitive to the PET calculation approach; we and Caracciolo et al. (2018) used PET equations from the same family, i.e., temperature-based formulations (Hamon, 1963; Thornthwaite, 1948, respectively).

Our projections indicate a future decrease in the overall CONUS ω, with a more substantial change at end-century under RCP 8.5 (ω = 2.43 (−5.8 %); Fig. 12). This means an overall shift in precipitation partitioning from ET to water yield for the same PET/P. The change in ω is consistent with the projected reduction in soil moisture across CONUS, enhancing water limitation (Fig. 8). While ω is known to be sensitive to changes in vegetation, and our simulations project significant changes in LAI in many regions (Fig. 7), the overall projected change in LAI (CONUS) is insignificant. Our results contrast with Heidari et al., (2021b). Based on VIC simulations driven with downscaled (MACA) CMIP5 climate projections from three GCMs representing wet, middle, and dry scenarios under RCP 8.5, they found little change in overall ω (CONUS) at end-century (2070–2099 vs. 1986–2015), with values of 2.135 (present), 2.162 (+1.3%, wet projection), 2.159 (+1.1%, mid projection), and 2.133 (−0.1%, dry projection). Among the differences in modeling approach that could explain the contrasting results, it is worth noting that Heidari et al., (2021b) calculated PET as Penman-Monteith open water ET (Shuttleworth, 1993, according to the VIC model description in Liang et al., 1994), while we used a temperature-based formulation (Hamon, 1963). As discussed earlier in this paper, Duan et al. (2017) have shown that the Hamon PET formulation in WaSSI leads to a stronger drying in response to increasing air temperature in comparison with the Penman-Monteith reference crop ET, noting that the latter method can account for the attenuation associated with increasing specific air humidity. The Penman-Monteith open water ET in the VIC model can do the same. An interesting point is that the Penman-Monteith open water ET values are typically larger than PET values obtained from other methods, as exemplified in Liang et al. (1994), who found Penman-Monteith open water ET values to be on average 1.64 times larger than Hamon's PET during an intensive field campaign in central Kansas. This offers an explanation for the generally lower ω values for CONUS reported by Heidari et al., (2021b), compared to our values and those in Caracciolo et al. (2018). In Fu's equation, considering fixed ET and P values, a larger PET value requires a lower ω value to compensate.

4.2. Drivers of water yield change

Our finding that climate change rather than land surface change dominates water yield change in CONUS is consistent with the recent results reported by Song et al. (2023) for China. They used a simple

hydrological model (Distributed Time-Variant Gain Model – Penman-Monteith-Leuning; Song et al., 2022), driven with climate and LAI data products from 1982 to 2012, to assess the relative contributions from climate change (*P*, PET) and land surface change (LAI) to water yield change**.** At the national level, Song et al. (2023) found that climate change made a substantially larger contribution to annual mean water yield (−7.6 mm) than land surface change (−0.6 mm). Interestingly, this is one order of magnitude lower than the climate change contribution, as we generally found in our study. However, unlike our study, they found substantial land surface contribution in particular regions, especially water-limited areas with substantial change in LAI. It is important to note that the assessment by Song et al. (2023) is based on observations (data products), reflecting not only "natural" changes in land surface cover (i.e., those in response to rising atmospheric CO_2 and climate change), but also direct anthropogenic land cover/land use changes, including the substantial "greening" associated with large-scale afforestation programs in China (Hu et al., 2021; Liu et al., 2014, 2016). Substantial impacts of direct anthropogenic changes in land cover/land use on water yield are also demonstrated in the urbanization study by Li et al. (2020) for CONUS, for instance. In a different study, Sun et al. (2015a) found an 8% increase in water yield in CONUS in response to a 50% decrease in LAI, in an WaSSI sensitivity test to simulate forest thinning. In our study, we only simulate the "natural" changes in land cover. It is also worth emphasizing that in our framework, the projected future land cover (LAI and vegetation type) at the HUC8 level is derived from present-day observations and ecoregion-level changes informed by MC2 simulations of potential vegetation. This approach allows us to capture larger scale patterns of vegetation change in our HUC8 projections, but not changes due to more localized climate conditions and natural disturbances. This contributes to a smoother vegetation change signal at the HUC8 scale, and consequently a smoother impact on local hydrology.

Our results contrast with those in Zhou et al. (2023). Based on CMIP6 output, including fully-coupled simulations with 16 GCMs and CO_2 sensitivity simulations with 7 GCMs, Zhou et al. (2023) found that the projected future changes in global water yield are mainly attributed to land surface change (73–81%), not climate change (19–27%). They found strong contributions from climate change at the regional level, but cancellation of positive and negative values led to a relatively small overall (global) contribution to water yield change. Even so, the reported effect of land surface change on water yield change is substantially larger than that in our study. It is important to note that the "land effect" in Zhou et al. (2023) encompasses not only the effect of change in land cover in response to climate change and rising atmospheric CO_2, but also the effect of change in stomatal conductance while land use change was not simulated. In our study, the "land effect" that we investigate is simply the impact of vegetation change (i.e., changes in LAI in response to climate change and increasing CO_2) on water yield change. To reduce the large uncertainty of the positive or negative effects of CO_2 and vapor pressure deficit on ET, WaSSI estimates ET with an empirical formulation, without an explicit representation of stomatal conductance and disregards the regulation of stomatal conductance by atmospheric CO_2. The absence of representation of the CO_2 effect on stomatal conductance is commonplace in water-centric model applications (e.g., Duan et al., 2017; Heidari et al., 2021a, 2021b; Song et al., 2023; Sun et al., 2016). Currently, the prevailing school of thought is that CO_2 fertilization reduces stomatal conductance (Li et al., 2023; Medlyn et al., 2001). In this sense, our projected future ET and water yield in CONUS could be potentially over- and underestimated, respectively, and our estimate of land contribution to water yield change could be underestimated by the lack of representation of the CO_2 effect on stomatal conductance. However, the impact of CO_2 fertilization on stomatal conductance is not a settled topic, with recent experimental studies challenging the prevailing idea of a widespread reduction in stomatal conductance with rising atmospheric CO_2 (Guerrieri et al., 2019; Mathias and Thomas, 2021). The results by Zhou et al. (2023) indicate a substantial contribution (54 %) from direct physiological effects (changes in vegetation cover and stomatal conductance in response to rising atmospheric CO_2) on global water yield change. These results reflect the structure of the considered CMIP6 GCMs, which despite substantial differences, generally follow the prevailing school of thought regarding the effects of CO_2 fertilization. As new studies based on long-term experiments become available, the modeling community will have valuable information to confirm or revisit the representation of CO_2 fertilization within GCMs.

4.3. Limitations and recommendations for future studies

Our modeling approach has some limitations. First, WaSSI simulates ET with an empirical formulation, without an explicit representation of stomatal conductance and disregarding its regulation by atmospheric CO_2 (common-place in water-centric model applications). Second, WaSSI simulates ET based on PET that is estimated with a temperature-based formulation (Hamon, 1963), which is unable to account for the projected increases in specific air humidity. Our projected increase in ET and decrease in water yield in CONUS could be overestimated due to these limitations. Also, our estimate of vegetation contribution to water yield change could be underestimated by the lack of representation of the CO_2 effect on stomatal conductance. It is important to point out that, while the simplicity of WaSSI and other water-centric models imposes some limitations, it also allows for less computationally expensive simulations, easier calibration, and implementation at finer spatio-temporal resolutions in comparison with mechanistic Terrestrial Biosphere Models. These models are much more computationally expensive to run and involve many parameters that oftentimes cannot be constrained by available observations and therefore can lead to substantial uncertainties in model simulations (Ma et al., 2022).

In future work, we recommend the use of a Penman-Monteith-based formulation for PET (and adapted ET equation for the chosen PET reference) within WaSSI if all required climate forcing data are available, as in Duan et al. (2017). Future work could explore ways to implement an empirical regulation factor in WaSSI's ET formulation to reflect stomatal response to atmospheric CO_2, although this regulation is a complex process depending on many biophysical and environmental factors that would be challenging to represent within a simple water-centric model. Future work could also test alternative projections of LAI and vegetation type within our proposed WaSSI-DGVM framework. The MC2 projections considered here indicate approximately neutral or negative LAI trends for most ecoregions in the twenty-first century, which could possibly indicate an overestimation of wildfire frequency and intensity by MC2. However, our results suggest that even modest adjustments in projected LAI are unlikely to change our finding that climate change dominates the projected changes in water yield. It is important to mention that here we focus on "natural" land cover change in response to changing climate and atmospheric CO_2, not anthropogenic land cover/land use change. The latter can exert a substantial impact on water yield. Future studies incorporating projections of anthropogenic changes in land cover/land use would be important contributions.

Finally, it is important to note that our study focused on classic future climate projections from CMIP5. While there have been some concerns that RCP 8.5 scenario may be implausibly too warm (Hausfather and Peters, 2020), we believe it still serves a useful role as a very high warming scenario. In fact, more recent projections from CMIP6 for CONUS indicate an even larger increase in surface air temperature at end-century (i.e., 2°–6°C and 4°–8°C under the Shared Socioeconomic Pathways (SSPs) 2-4.5 and 5-8.5, respectively; 2075–2099 relative to 1970–1999; Fan et al., 2020) compared to CMIP5 (1.3°–3.7 °C and 3.0°–6.1 °C under RCPs 4.5 and 8.5, respectively; 2070–2099 relative to 1986–2015; Hayhoe et al., 2018). Projected changes in annual precipitation under SSP 2-4.5 (5-8.5) have a similar overall spatial pattern in CONUS compared to RCP 4.5 (8.5), but tend to be shifted towards

Table A1
Crosswalk between MC2 and WaSSI natural vegetation types.

v (MC2)	Description	*v* (WaSSI)	Desc.[a]
0	UNKNOWNveg	–	UN
1	COLD_BARRENveg	6	BA
2	TUNDRAveg	6	BA
3	TAIGA_TUNDRAveg	2	ET
4	BOREAL_NEEDLELEAF_FORESTveg	2	ET
5	BOREAL_WOODLANDveg	2	ET
6	SUBALPINE_FORESTveg	2	ET
7	MARITIME_EN_FORESTveg	2	ET
8	MESIC_TEMPERATE_NEEDLELEAF_FORESTveg	2	ET
9	TEMPERATE_DB_FORESTveg	1	DT
10	COOL_MIXED_FORESTveg	3	MT
11	TEMPERATE_WARM_MIXED_FORESTveg	3	MT
12	TEMPERATE_EN_WOODLANDveg	2	ET
13	TEMPERATE_DB_WOODLANDveg	1	DT
14	TEMPERATE_COOL_MIXED_WOODLANDveg	3	MT
15	TEMPERATE_WARM_MIXED_WOODLANDveg	3	MT
16	C3SHRUBveg	4	SH
17	C3GRASSveg	5	GR
18	TEMPERATE_DESERTveg	6	BA
19	SUBTROPICAL_EN_FORESTveg	2	ET
20	SUBTROPICAL_DB_FORESTveg	1	DT
21	WARM_EB_FORESTveg	2	ET
22	SUBTROPICAL_MIXED_FORESTveg	3	MT
23	SUBTROPICAL_EN_WOODLANDveg	2	ET
24	SUBTROPICAL_DB_WOODLANDveg	1	DT
25	SUBTROPICAL_EB_WOODLANDveg	2	ET
26	SUBTROPICAL_MIXED_WOODLANDveg	3	MT
27	C4SHRUBveg	4	SH
28	C4GRASSveg	5	GR
29	SUBTROPICAL_DESERTveg	6	BA
30	TROPICAL_EB_FORESTveg	2	ET
31	TROPICAL_DECIDUOUS_WOODLANDveg	1	DT
32	TROPICAL_SAVANNAveg	5	GR
35	TROPICAL_DESERTveg	6	BA
36	MOIST_TEMPERATE_NEEDLELEAF_FORESTveg	2	ET
38	SUBALPINE_MEADOWveg	5	GR
39	WATERveg	–	UN
40	NATURAL_BARRENveg	6	BA
49	DRY_TEMPERATE_NEEDLELEAF_FORESTveg	2	ET
50	XERIC_NEEDLELEAF_WOODLANDveg	2	ET

[a] Deciduous forest (DT), evergreen forest (ET), mixed forest (MT), shrubland (SH), grassland (GR), barren (BA), undefined (UN).

positive values (i.e., larger increases and smaller decreases in precipitation; Du et al., 2022). Climate extreme indicators such as the annual peak of daily maximum temperature and the number of heavy precipitation days are generally more accentuated in SSP 2-4.5 and 5-8.5 than in RCP 4.5 and 8.5 at end-century in CONUS (Chen et al., 2020). While the warmer conditions predicted by the CMIP6 GCMs would contribute to increased ET and decreased water yield, the wetter conditions would contribute to increased water yield. While SSP 3-7.0 may serve as an alternative high warming scenario, some caution that it represents a special aerosol emissions case and should be accompanied by SSP 5-8.5 (Shiogama et al., 2023). Future work exploring the impact of the new CMIP6 climate projections on vegetation dynamics and hydrology with the WaSSI-MC2 framework would be an important advance.

5. Conclusions

This study integrated an eco-hydrological model (WaSSI) with a large ensemble of climate (LOCA) and vegetation (MC2 DGVM) projections under scenarios RCP 4.5 and 8.5 to investigate potential future impacts of both climate and vegetation change on water yield. To our knowledge, this is the first work to employ an ensemble of future vegetation projections and provide water yield projections for CONUS at a relatively fine scale (HUC8).

We project a decrease in water yield across much of CONUS, especially towards the end of the twenty-first century (2080–2099) under RCP 8.5. Overall, our projected water yield reduction under RCP 8.5 is roughly twice as high as under RCP 4.5. We project substantial changes in water yield for watersheds in the central and southeastern U.S. already by mid-century (2040–2059). We conclude that climate change (air temperature, precipitation), rather than vegetation change (LAI), strongly dominates the projected changes in water yield. For some watersheds, the effects of vegetation change can be relevant, mitigating or exacerbating the effects of climate change. Our future projections indicate widespread increase in aridity (PET/*P*) and evaporative (ET/*P*) indices and widespread decrease in soil moisture under both RCP scenarios, but especially under RCP 8.5.

Our integrated modeling results can inform policy makers and resource development planners quantitative information of future water availability under contrasting scenarios. We point out regions under higher risk of future water shortages that may affect water supply to both human and ecosystems. Land managers may need to consider new management regimes or approaches in basins identified as having declining water supply and soil moisture, as these may be more prone to wildfires and insect outbreaks. Conversely, our projections can be used to quantify the substantial benefits of climate change mitigation (scenario RCP 4.5 vs. 8.5) to the U.S. water supply.

Funding

This study was funded by the USDA Southeast Climate Hub and Forest Service Southern Research Station under Joint Venture Agreement 21-JV-11330180–049. J.X. was also supported by the National Science Foundation (Macrosystems Biology and NEON-Enabled Science Program: DEB-2017870). This study was also jointly supported by the Eastern and Western Threat Assessment Centers of the USDA Forest Service.

CRediT authorship contribution statement

Henrique F. Duarte: Writing – original draft, Visualization, Software, Methodology, Investigation, Formal analysis, Data curation, Conceptualization. **John B. Kim:** Writing – review & editing, Resources, Methodology, Conceptualization. **Ge Sun:** Writing – review & editing, Resources, Project administration, Methodology, Funding acquisition, Conceptualization. **Steven McNulty:** Writing – review & editing, Project administration, Methodology, Funding acquisition, Conceptualization. **Jingfeng Xiao:** Writing – review & editing, Project administration, Methodology, Funding acquisition, Conceptualization.

Data availability

The downscaled CMIP5 climate projections (LOCA) are available in Pierce (2024). PRISM meteorological data are available in PRISM Climate Group (2024). MODIS ET data are available in Running et al. (2021). The MC2 DGVM model code is available in USDA FS (2022). The MC2 projections of potential vegetation (vegetation type and LAI), our WaSSI projections of water yield, ET, and soil moisture, and the adapted WaSSI model code used in our investigation can be downloaded from http://globalecology.unh.edu/data.html.

Declaration of competing interest

The authors declare that they have no known competing financial interests or personal relationships that could have appeared to influence the work reported in this paper.

Appendix A. Dynamic vegetation boundary conditions within WaSSI

We started with MC2 simulations of potential natural vegetation across CONUS, with annual outputs (1950–2005 and 2006–2099 under scenarios RCP 4.5 and 8.5) of vegetation type and corresponding LAI at the 1/16° spatial scale. We considered an ensemble of MC2 simulations, driven by statistically downscaled climate simulations from 16 GCMs (LOCA; Pierce et al., 2015, 2014; see Table 1).

We calculated LAI as the sum of the MC2 output variables MAX_GRASS_LAI and MAX_TREE_LAI and translated the original vegetation types (up to 50) to one of the six natural vegetation types in WaSSI (deciduous forest, evergreen forest, mixed forest, shrubland, grassland, and barren), following the crosswalk presented in Table A1.

We used the 2006 NLCD data product (USGS, 2011) to create a mask of natural vegetation areas for the MC2 output, masking out areas characterized by other land cover types (e.g., developed areas, croplands, and artificial pasture). To create the mask, we aggregated the original 30-m spatial resolution NLCD data at the 1/16° spatial scale (MC2 output grid), using the mode as the representative value.

Next, we aggregated the masked MC2 output at the ecoregion level (level-2 ecoregions of North America, EPA, 2010; Fig. 3). We calculated the area fraction (f_{MC2}) of vegetation type v (6 possible natural vegetation types) within ecoregion e (20 possible ecoregions) for year y (1950–2099) as

$$f_{\mathrm{MC2}(y,e,v)} = \frac{A_{y,e,v}}{\sum_{j=1}^{6} A_{y,e,j}} \tag{A.1}$$

where $A_{y,e,v}$ is the total area of vegetation type v within the ecoregion e for year y. The denominator of Eq. (A.1) represents the total natural vegetation area within the ecoregion, in which j is an auxiliary index. We also calculated the overall LAI (LAI_{MC2}) of vegetation type v for ecoregion e and year y as

$$\mathrm{LAI}_{\mathrm{MC2}(y,e,v)} = \frac{\sum_{i=1}^{n} \left(\mathrm{lai}_{y,e,v,i}\ a_{y,e,v,i}\right)}{\sum_{i=1}^{n} a_{y,e,v,i}} \tag{A.2}$$

where $\mathrm{lai}_{y,e,v,i}$ and $a_{y,e,v,i}$ are the LAI and area of individual (i) grid cells of vegetation type v within ecoregion e for year y, respectively, and n is the number of grid cells.

For each vegetation type v and ecoregion e, we defined baselines of area fraction ($\widehat{f}_{MC2}$) and LAI ($\widehat{\mathrm{LAI}}_{MC2}$) as

$$\widehat{f}_{\mathrm{MC2}(e,v)} = \frac{1}{y_{\mathrm{fin}} - y_{\mathrm{ini}} + 1} \sum_{y=y_{\mathrm{ini}}}^{y_{\mathrm{fin}}} f_{\mathrm{MC2}(y,e,v)} \tag{A.3}$$

$$\widehat{\mathrm{LAI}}_{\mathrm{MC2}(e,v)} = \frac{1}{y_{\mathrm{fin}} - y_{\mathrm{ini}} + 1} \sum_{y=y_{\mathrm{ini}}}^{y_{\mathrm{fin}}} \mathrm{LAI}_{\mathrm{MC2}(y,e,v)} \tag{A.4}$$

where $\left[y_{\mathrm{ini}} : y_{\mathrm{fin}}\right]$ is the chosen period of reference, here taken as [2000 : 2006].

For each vegetation type v, ecoregion e, and year y (2007–2099), we calculated the area fraction and LAI deviations from baseline (Δf_{MC2} and $\Delta\mathrm{LAI}_{MC2}$, respectively) as

$$\Delta f_{\mathrm{MC2}(y,e,v)} = f_{\mathrm{MC2}(y,e,v)} - \widehat{f}_{\mathrm{MC2}(e,v)} \tag{A.5}$$

$$\Delta\mathrm{LAI}_{\mathrm{MC2}(y,e,v)} = \frac{\mathrm{LAI}_{\mathrm{MC2}(y,e,v)} - \widehat{\mathrm{LAI}}_{\mathrm{MC2}(e,v)}}{\widehat{\mathrm{LAI}}_{\mathrm{MC2}(e,v)}} \tag{A.6}$$

These deviations were combined with "present-day observations" (data products) to create projections of land cover type and LAI to drive WaSSI.

WaSSI considers a total of 10 land cover types, which includes the 6 natural vegetation types discussed earlier (deciduous forest, evergreen forest, mixed forest, shrubland, grassland, and barren) in addition to urban, cropland, wetland, and water types. WaSSI provides input datasets for CONUS describing the area fraction of each land cover type c within HUC8s (h), $\widehat{f}_{\mathrm{OBS}(h,c)}$, and the associated monthly (m) LAI, $\widehat{\mathrm{LAI}}_{\mathrm{OBS}(m,h,c)}$. These default input datasets were built based on the 2006 NLCD (USGS, 2011) and 2000–2006 mean monthly MODIS LAI (Zhao et al., 2005). We combined $\widehat{f}_{\mathrm{OBS}}$ with Δf_{MC2} to project the area fraction of vegetation type v within HUC8 h for year y, $f_{\mathrm{WaSSI}(y,h,v)}$, as

$$f_{\mathrm{WaSSI}(y,h,v)} = \frac{X_{y,h,v}}{\sum_{k=1}^{6} X_{y,h,k}} \sum_{j=1}^{6} \widehat{f}_{\mathrm{OBS}(h,j)} \tag{A.7}$$

where X is the unnormalized area fraction of vegetation type v relative to the total natural vegetation area within HUC8 h projected for year y

$$X_{y,h,v} = \frac{\widehat{f}_{\mathrm{OBS}(h,v)}}{\sum_{j=1}^{6} \widehat{f}_{\mathrm{OBS}(h,j)}} + \Delta f_{\mathrm{MC2}(y,e(h),v)} \tag{A.8}$$

In Eqs. (A.7) and (A.8), j and k are auxiliary indices, with summations defined across the six natural vegetation types ($v[1:6]$, which corresponds to $c[1:6]$ in our notation). X values are truncated to [0 : 1]. Note that X is normalized in Eq. (A.7) to enforce that $\sum_{j=1}^{6} f_{\mathrm{WaSSI}(y,h,j)}$ is equal to $\sum_{j=1}^{6} \widehat{f}_{\mathrm{OBS}(h,j)}$, i.e., the natural vegetation area fraction of the HUC8 h based on "present-day observations", which remains constant in our projections as we do not simulate land use change (urban, cropland, wetland, and water fractions are constant in time). Note also that in Eq. (A.8), the index $e(h)$ denotes the ecoregion e associated with the HUC8 h. Finally, we combined $\widehat{\mathrm{LAI}}_{\mathrm{OBS}}$ with $\Delta\mathrm{LAI}_{MC2}$ to project the monthly (m) LAI for vegetation type v in HUC8 h for year y, $\mathrm{LAI}_{\mathrm{WaSSI}(y,m,h,v)}$, as

$$\mathrm{LAI}_{\mathrm{WaSSI}(y,m,h,v)} = \widehat{\mathrm{LAI}}_{\mathrm{OBS}(m,h,v)}\left(1 + \Delta\mathrm{LAI}_{\mathrm{MC2}(y,e(h),v)}\right) \quad \text{(A.9)}$$

For the instances in which $\Delta\mathrm{LAI}_{\mathrm{MC2}}$ was undefined, we assumed it to be zero. For the instances in which $\widehat{\mathrm{LAI}}_{\mathrm{OBS}}$ was undefined, we used a monthly (m) area-weighted averaged observed LAI for vegetation type v within the ecoregion encompassing HUC8 h. If still undefined, we expanded the averaging domain to the entire CONUS.

Appendix B. Supplementary data

Figures S1 to S5 are included in the Supplement S1 [R1-Supplement-S1.pdf]. Supplementary data to this article can be found online at https://doi.org/10.1016/j.jhydrol.2024.131472.

References

Abatzoglou, J.T., Brown, T.J., 2012. A comparison of statistical downscaling methods suited for wildfire applications. Int. J. Climatol. 32, 772–780.

Allen, R.G., Pereira, L.S., Raes, D., Smith, M., 1998. Crop evapotranspiration - Guidelines for computing crop water requirements - FAO irrigation and drainage paper 56. FAO, Rome, Italy.

Al-Qubati, A., Zhang, L., Pyarali, K., 2023. Climatic drought impacts on key ecosystem services of a low mountain region in Germany. Environ. Monit. Assess. 195, 800.

Bachelet, D., Lenihan, J.M., Daly, C., Neilson, R.P., Ojima, D.S., Parton, W.J., 2001. MC1: a dynamic vegetation model for estimating the distribution of vegetation and associated carbon, nutrients, and water — technical documentation. Version 1.0. Gen. Tech. Rep. PNW-GTR-508. U.S. Department of Agriculture, Forest Service, Pacific Northwest Research Station, Portland, USA.

Bagstad, K.J., Cohen, E., Ancona, Z.H., McNulty, S.G., Sun, G., 2018. The sensitivity of ecosystem service models to choices of input data and spatial resolution. Appl. Geogr. 93, 25–36.

Beck, H.E., McVicar, T.R., Vergopolan, N., Berg, A., Lutsko, N.J., Dufour, A., Zeng, Z., Jiang, X., van Dijk, A.I.J.M., Miralles, D.G., 2023. High-resolution (1 km) Köppen-Geiger maps for 1901–2099 based on constrained CMIP6 projections. Sci. Data 10, 724.

Bellouin, N., Collins, W.J., Culverwell, I.D., Halloran, P.R., Hardiman, S.C., Hinton, T.J., Jones, C.D., McDonald, R.E., McLaren, A.J., O'Connor, F.M., Roberts, M.J., Rodriguez, J.M., Woodward, S., Best, M.J., Brooks, M.E., Brown, A.R., Butchart, N., Dearden, C., Derbyshire, S.H., Dharssi, I., Doutriaux-Boucher, M., Edwards, J.M., Falloon, P.D., Gedney, N., Gray, L.J., Hewitt, H.T., Hobson, M., Huddleston, M.R., Hughes, J., Ineson, S., Ingram, W.J., James, P.M., Johns, T.C., Johnson, C.E., Jones, A., Jones, C.P., Joshi, M.M., Keen, A.B., Liddicoat, S., Lock, A.P., Maidens, A. V., Manners, J.C., Milton, S.F., Rae, J.G.L., Ridley, J.K., Sellar, A., Senior, C.A., Totterdell, I.J., Verhoef, A., Vidale, P.L., Wiltshire, A., 2011. The HadGEM2 family of Met Office Unified Model climate configurations. Geosci. Model Dev. 4, 723–757.

Bentsen, M., Bethke, I., Debernard, J.B., Iversen, T., Kirkevåg, A., Seland, Ø., Drange, H., Roelandt, C., Seierstad, I.A., Hoose, C., Kristjánsson, J.E., 2013. The Norwegian Earth System Model, NorESM1-M – Part 1: Description and basic evaluation of the physical climate. Geosci. Model Dev. 6, 687–720.

Berg, A., Sheffield, J., Milly, P.C.D., 2017. Divergent surface and total soil moisture projections under global warming. Geophys. Res. Lett. 44, 236–244.

Bi, D., Dix, M., Marsland, S., O'Farrell, S., Rashid, H., Uotila, P., Hirst, A., Kowalczyk, E., Golebiewski, M., Sullivan, A., Yan, H., Hannah, N., Franklin, C., Sun, Z., Vohralik, P., Watterson, I., Zhou, X., Fiedler, R., Collier, M., Ma, Y., Noonan, J., Stevens, L., Uhe, P., Zhu, H., Griffies, S., Hill, R., Harris, C., Puri, K., 2013. The ACCESS coupled model: description, control climate and evaluation. Aust. Meteorol. Oceanogr. J. 63, 41–64.

Brown, T.C., Mahat, V., Ramirez, J.A., 2019. Adaptation to Future Water Shortages in the United States Caused by Population Growth and Climate Change. Earths Future 7, 219–234.

Budyko, M.I., 1958. The heat balance of the Earth's surface (translation by N.A. Stepanova). U.S. Department of Commerce/ Weather Bureau, Washington, USA.

Burnash, R.J.C., 1995. The NWS river forecast system - catchment modeling. In: Singh, V. P. (Ed.), Computer Models of Watershed Hydrology. Water Resources Publications, Littleton, CO, USA, pp. 311–366.

Burnash, R.J.C., Ferral, R.L., McGuire, R.A., 1973. A generalized streamflow simulation system - Conceptual modeling for digital computers. U.S. National Weather Service and California Department of Water Resources, Sacramento, USA.

Caldwell, P.V., Sun, G., McNulty, S.G., Cohen, E.C., Moore Myers, J.A., 2012. Impacts of impervious cover, water withdrawals, and climate change on river flows in the conterminous US. Hydrol. Earth Syst. Sci. 16, 2839–2857.

Caracciolo, D., Pumo, D., Viola, F., 2018. Budyko's Based Method for Annual Runoff Characterization across Different Climatic Areas: an Application to United States. Water Resour. Manag. 32, 3189–3202.

Chen, H., Sun, J., Lin, W., Xu, H., 2020. Comparison of CMIP6 and CMIP5 models in simulating climate extremes. Sci Bull (beijing) 65, 1415–1418.

Cherkauer, K.A., Bowling, L.C., Lettenmaier, D.P., 2003. Variable infiltration capacity cold land process model updates. Glob Planet Change 38, 151–159.

Chylek, P., Li, J., Dubey, M.K., Wang, M., Lesins, G., 2011. Observed and model simulated 20th century Arctic temperature variability: Canadian Earth System Model CanESM2. Atmos. Chem. Phys. Discuss. 11, 22893–22907.

Conklin, D.R., Lenihan, J.M., Bachelet, D., Neilson, R.P., Kim, J.B., 2016. MCFire model technical description. Gen. Tech. Rep. PNW-GTR-926. U.S. Department of Agriculture, Forest Service, Pacific Northwest Research Station, Portland, USA.

Donner, L.J., Wyman, B.L., Hemler, R.S., Horowitz, L.W., Ming, Y., Zhao, M., Golaz, J.-C., Ginoux, P., Lin, S.-J., Schwarzkopf, M.D., Austin, J., Alaka, G., Cooke, W.F., Delworth, T.L., Freidenreich, S.M., Gordon, C.T., Griffies, S.M., Held, I.M., Hurlin, W.J., Klein, S.A., Knutson, T.R., Langenhorst, A.R., Lee, H.-C., Lin, Y., Magi, B.I., Malyshev, S.L., Milly, P.C.D., Naik, V., Nath, M.J., Pincus, R., Ploshay, J. J., Ramaswamy, V., Seman, C.J., Shevliakova, E., Sirutis, J.J., Stern, W.F., Stouffer, R.J., Wilson, R.J., Winton, M., Wittenberg, A.T., Zeng, F., 2011. The Dynamical Core, Physical Parameterizations, and Basic Simulation Characteristics of the Atmospheric Component AM3 of the GFDL Global Coupled Model CM3. J. Clim. 24, 3484–3519.

Du, Y., Wang, D., Zhu, J., Wang, D., Qi, X., Cai, J., 2022. Comprehensive assessment of CMIP5 and CMIP6 models in simulating and projecting precipitation over the global land. Int. J. Climatol. 42, 6859–6875.

Duan, K., Sun, G., McNulty, S.G., Caldwell, P.V., Cohen, E.C., Sun, S., Aldridge, H.D., Zhou, D., Zhang, L., Zhang, Y., 2017. Future shift of the relative roles of precipitation and temperature in controlling annual runoff in the conterminous United States. Hydrol. Earth Syst. Sci. 21, 5517–5529.

Duan, K., Caldwell, P.V., Sun, G., McNulty, S.G., Zhang, Y., Shuster, E., Liu, B., Bolstad, P. V., 2019. Understanding the role of regional water connectivity in mitigating climate change impacts on surface water supply stress in the United States. J Hydrol (amst) 570, 80–95.

Dufresne, J.-L., Foujols, M.-A., Denvil, S., Caubel, A., Marti, O., Aumont, O., Balkanski, Y., Bekki, S., Bellenger, H., Benshila, R., Bony, S., Bopp, L., Braconnot, P., Brockmann, P., Cadule, P., Cheruy, F., Codron, F., Cozic, A., Cugnet, D., de Noblet, N., Duvel, J.-P., Ethé, C., Fairhead, L., Fichefet, T., Flavoni, S., Friedlingstein, P., Grandpeix, J.-Y., Guez, L., Guilyardi, E., Hauglustaine, D., Hourdin, F., Idelkadi, A., Ghattas, J., Joussaume, S., Kageyama, M., Krinner, G., Labetoulle, S., Lahellec, A., Lefebvre, M.-P., Lefevre, F., Levy, C., Li, Z.X., Lloyd, J., Lott, F., Madec, G., Mancip, M., Marchand, M., Masson, S., Meurdesoif, Y., Mignot, J., Musat, I., Parouty, S., Polcher, J., Rio, C., Schulz, M., Swingedouw, D., Szopa, S., Talandier, C., Terray, P., Viovy, N., Vuichard, N., 2013. Climate change projections using the IPSL-CM5 Earth System Model: from CMIP3 to CMIP5. Clim. Dyn. 40, 2123–2165.

Dunne, J.P., John, J.G., Adcroft, A.J., Griffies, S.M., Hallberg, R.W., Shevliakova, E., Stouffer, R.J., Cooke, W., Dunne, K.A., Harrison, M.J., Krasting, J.P., Malyshev, S.L., Milly, P.C.D., Phillipps, P.J., Sentman, L.T., Samuels, B.L., Spelman, M.J., Winton, M., Wittenberg, A.T., Zadeh, N., 2012. GFDL's ESM2 Global Coupled Climate-Carbon Earth System Models. Part I: Physical Formulation and Baseline Simulation Characteristics. J. Clim. 25, 6646–6665.

Easterling, D.R., Kunkel, K.E., Arnold, J.R., Knutson, T., LeGrande, A.N., Leung, L.R., Vose, R.S., Waliser, D.E., Wehner, M.F., 2017. Precipitation change in the United States. In: Wuebbles, D., Fahey, D.W., Hibbard, K.A., Dokken, D.J., Stewart, B.C., Maycock, T.K. (Eds.), Climate Science Special Report: Fourth National Climate Assessment, vol. I. U.S. Global Change Research Program, Washington, DC, USA, pp. 207–230.

EPA, 2010. Ecoregions: Level II ecoregions of North America, NA_CEC_Eco_Level2 (vector digital data) [dataset]. U.S. EPA Office of Research and Development (ORD) - National Health and Environmental Effects Research Laboratory (NHEERL), Corvallis, USA.

EPA, 2017. Multi-model framework for quantitative sectoral impacts analysis: a technical report for the Fourth National Climate Assessment (EPA 430-R-17-001). U.S. Environmental Protection Agency.

Fan, X., Duan, Q., Shen, C., Wu, Y., Xing, C., 2020. Global surface air temperatures in CMIP6: historical performance and future changes. Environ. Res. Lett. 15, 104056.

Fang, K., Shen, C., Fisher, J.B., Niu, J., 2016. Improving Budyko curve-based estimates of long-term water partitioning using hydrologic signatures from GRACE. Water Resour. Res. 52, 5537–5554.

USDA FS, 2022. MC2 Dynamic Global Vegetation Model, v2.124 [WWW Document]. https://doi.org/10.5281/zenodo.7470678.

Fu, B., 1981. On the calculation of the evaporation from land surface. Scientia Atmospherica Sinica 5, 23–31.

Gent, P.R., Danabasoglu, G., Donner, L.J., Holland, M.M., Hunke, E.C., Jayne, S.R., Lawrence, D.M., Neale, R.B., Rasch, P.J., Vertenstein, M., Worley, P.H., Yang, Z.-L., Zhang, M., 2011. The Community Climate System Model Version 4. J. Clim. 24, 4973–4991.

Golub, A., Sohngen, B., Cai, Y., Kim, J., Hertel, T., 2022. Costs of forest carbon sequestration in the presence of climate change impacts. Environ. Res. Lett. 17, 104011.
Gonzalez, P., Neilson, R.P., Lenihan, J.M., Drapek, R.J., 2010. Global patterns in the vulnerability of ecosystems to vegetation shifts due to climate change. Glob. Ecol. Biogeogr. 19, 755–768.
Grimm, N.B., Chapin, F.S., Bierwagen, B., Gonzalez, P., Groffman, P.M., Luo, Y., Melton, F., Nadelhoffer, K., Pairis, A., Raymond, P.A., Schimel, J., Williamson, C.E., 2013. The impacts of climate change on ecosystem structure and function. Front. Ecol. Environ. 11, 474–482.
Guerrieri, R., Belmecheri, S., Ollinger, S. V., Asbjornsen, H., Jennings, K., Xiao, J., Stocker, B.D., Martin, M., Hollinger, D.Y., Bracho-Garrillo, R., Clark, K., Dore, S., Kolb, T., Munger, J.W., Novick, K., Richardson, A.D., 2019. Disentangling the role of photosynthesis and stomatal conductance on rising forest water-use efficiency. Proceedings of the National Academy of Sciences 116, 16909–16914. https://doi.org/10.1073/pnas.1905912116.
Hamon, W.R., 1963. Computation of direct runoff amounts from storm rainfall. International Association of Scientific Hydrology 63, 52–62.
Hausfather, Z., Peters, G.P., 2020. RCP8.5 is a problematic scenario for near-term emissions. Proc. National Acad. Sci. 117, 27791–27792.
Hayhoe, K., Wuebbles, D., Easterling, D.R., Fahey, D.W., Doherty, S., Kossin, J., Sweet, W., Vose, R., Wehner, M., 2018. Our changing climate. In: Reidmiller, D.R., Avery, C.W., Easterling, D.R., Kunkel, K.E., Lewis, K.L.M., Maycock, T.K., Stewart, B. C. (Eds.), Impacts, Risks, and Adaptation in the United States: Fourth National Climate Assessment, Volume II. USA, U.S, Global Change Research Program, Washington, DC, pp. 72–144.
Heidari, H., Arabi, M., Warziniack, T., 2021a. Vulnerability to Water Shortage Under Current and Future Water Supply-Demand Conditions Across U.S. River Basins. Earths Future 9.
Heidari, H., Warziniack, T., Brown, T.C., Arabi, M., 2021b. Impacts of Climate Change on Hydroclimatic Conditions of U.S. National Forests and Grasslands. Forests 12, 139.
Hu, J., Wu, Y., Wang, L., Sun, P., Zhao, F., Jin, Z., Wang, Y., Qiu, L., Lian, Y., 2021. Impacts of land-use conversions on the water cycle in a typical watershed in the southern Chinese Loess Plateau. J Hydrol (amst) 593, 125741.
Joo, J., Jeong, S., Zheng, C., Park, C.-E., Park, H., Kim, H., 2020. Emergence of significant soil moisture depletion in the near future. Environ. Res. Lett. 15, 124048.
Kerns, B.K., Kim, J.B., Kline, J.D., Day, M.A., 2016. US exposure to multiple landscape stressors and climate change. Reg. Environ. Chang. 16, 2129–2140.
Kim, J.B., Monier, E., Sohngen, B., Pitts, G.S., Drapek, R., McFarland, J., Ohrel, S., Cole, J., 2017. Assessing climate change impacts, benefits of mitigation, and uncertainties on major global forest regions under multiple socioeconomic and emissions scenarios. Environ. Res. Lett. 12, 045001.
Kim, J.B., Kerns, B.K., Drapek, R.J., Pitts, G.S., Halofsky, J.E., 2018. Simulating vegetation response to climate change in the Blue Mountains with MC2 dynamic global vegetation model. Clim. Serv. 10, 20–32.
Li, C., Sun, G., Caldwell, P.V., Cohen, E., Fang, Y., Zhang, Y., Oudin, L., Sanchez, G.M., Meentemeyer, R.K., 2020. Impacts of urbanization on watershed water balances across the conterminous United States. Water Resour. Res. 56, 1–19.
Li, F., Xiao, J., Chen, J., Ballantyne, A., Jin, K., Li, B., Abraha, M., John, R., 2023. Global water use efficiency saturation due to increased vapor pressure deficit. Science 1979 (381), 672–677.
Liang, X., Lettenmaier, D.P., Wood, E.F., Burges, S.J., 1994. A simple hydrologically based model of land surface water and energy fluxes for general circulation models. J. Geophys. Res. Atmos. 99, 14415–14428.
Liang, X., Wood, E.F., Lettenmaier, D.P., 1996. Surface soil moisture parameterization of the VIC-2L model: Evaluation and modification. Glob Planet Change 13, 195–206.
Liu, D., Chen, Y., Cai, W., Dong, W., Xiao, J., Chen, J., Zhang, H., Xia, J., Yuan, W., 2014. The contribution of China's Grain to Green Program to carbon sequestration. Landsc. Ecol. 29, 1675–1688.
Liu, N., Sun, P.-S., Liu, S.-R., Sun, G., 2013. Coupling simulation of water-carbon processes for catchment-calibration and validation of the WaSSI-C model. Chinese Journal of Plant Ecology 37, 492–502.
Liu, Y., Xiao, J., Ju, W., Xu, K., Zhou, Y., Zhao, Y., 2016. Recent trends in vegetation greenness in China significantly altered annual evapotranspiration and water yield. Environ. Res. Lett. 11, 094010.
Livneh, B., Rosenberg, E.A., Lin, C., Nijssen, B., Mishra, V., Andreadis, K.M., Maurer, E. P., Lettenmaier, D.P., 2013. A Long-Term Hydrologically Based Dataset of Land Surface Fluxes and States for the Conterminous United States: Update and Extensions. J. Clim. 26, 9384–9392.
Ma, R., Xiao, J., Liang, S., Ma, H., He, T., Guo, D., Liu, X., Lu, H., 2022. Pixel-level parameter optimization of a terrestrial biosphere model for improving estimation of carbon fluxes with an efficient model–data fusion method and satellite-derived LAI and GPP data. Geosci. Model Dev. 15, 6637–6657.
Mahat, V., Ramírez, J.A., Brown, T.C., 2017. Twenty-First-Century Climate in CMIP5 Simulations: Implications for Snow and Water Yield across the Contiguous United States. J. Hydrometeorol. 18, 2079–2099.
Mahowald, N., Lo, F., Zheng, Y., Harrison, L., Funk, C., Lombardozzi, D., Goodale, C., 2016. Projections of leaf area index in earth system models. Earth Syst. Dyn. 7, 211–229.
Mathias, J.M., Thomas, R.B., 2021. Global tree intrinsic water use efficiency is enhanced by increased atmospheric CO_2 and modulated by climate and plant functional types. Proc. National Acad. Sci. 118.
Medlyn, B.E., Barton, C.V.M., Broadmeadow, M.S.J., Ceulemans, R., De Angelis, P., Forstreuter, M., Freeman, M., Jackson, S.B., Kellomäki, S., Laitat, E., Rey, A., Roberntz, P., Sigurdsson, B.D., Strassemeyer, J., Wang, K., Curtis, P.S., Jarvis, P.G., 2001. Stomatal conductance of forest species after long-term exposure to elevated CO_2 concentration: a synthesis. New Phytol. 149, 247–264.
Mekonnen, Z.A., Riley, W.J., 2023. Climate Change Will Increase Biomass Proportion of Global Forest Carbon Stocks Under an SSP5–8.5 Climate Trajectory. Geophys. Res. Lett. 50.
Naz, B.S., Kao, S.-C., Ashfaq, M., Rastogi, D., Mei, R., Bowling, L.C., 2016. Regional hydrologic response to climate change in the conterminous United States using high-resolution hydroclimate simulations. Glob Planet Change 143, 100–117.
Neilson, R.P., 1995. A Model for Predicting Continental-Scale Vegetation Distribution and Water Balance. Ecol. Appl. 5, 362–385.
Nrcs, 2024. The Digital General Soil Map of the United States (STATSGO2), Natural Resources Conservation Service, United States Department of Agriculture [WWW Document]. accessed 2.3.24. .
Oudin, L., Andréassian, V., Lerat, J., Michel, C., 2008. Has land cover a significant impact on mean annual streamflow? An international assessment using 1508 catchments. J Hydrol (amst) 357, 303–316.
Parton, W.J., Scurlock, J.M.O., Ojima, D.S., Gilmanov, T.G., Scholes, R.J., Schimel, D.S., Kirchner, T., Menaut, J., Seastedt, T., Garcia Moya, E., Kamnalrut, A., Kinyamario, J. I., 1993. Observations and modeling of biomass and soil organic matter dynamics for the grassland biome worldwide. Global Biogeochem. Cycles 7, 785–809.
Pierce, D.W., Cayan, D.R., Thrasher, B.L., 2014. Statistical Downscaling Using Localized Constructed Analogs (LOCA). J. Hydrometeorol. 15, 2558–2585.
Pierce, D.W., Cayan, D.R., Maurer, E.P., Abatzoglou, J.T., Hegewisch, K.C., 2015. Improved Bias Correction Techniques for Hydrological Simulations of Climate Change. J. Hydrometeorol. 16, 2421–2442.
Pierce, D.W., 2024. LOCA Statistical Downscaling (Localized Constructed Analogs) - Statistically downscaled CMIP5 and CMIP6 climate projections for North America [WWW Document]. URL https://loca.ucsd.edu/ (accessed 1.15.24).
PRISM Climate Group, 2024. PRISM Gridded Climate Data, PRISM Climate Group, Oregon State University [dataset] [WWW Document]. URL https://prism.oregonstate.edu (accessed 4.24.24).
Reyer, C., Chang, J., Chen, M., Forrest, M., François, L., Henrot, A.-J., Hickler, T., Ito, A., Nishina, K., Ostberg, S., Schaphoff, S., Seneviratne, S.I., Shi, H., Steinkamp, J., Thiery, W., Tian, H., Zhao, F., Büchner, M., Ciais, P., 2019. ISIMIP2b Simulation Data from Biomes Sector, GFZ Data Services [dataset] [WWW Document]. https://doi.org/10.5880/PIK.2019.012.
Running, S., Mu, Q., Zhao, M., Moreno, A., 2021. MODIS/Terra Net Evapotranspiration Gap-Filled Yearly L4 Global 500m SIN Grid V061. NASA EOSDIS Land Processes Distributed Active Archive Center.
Shiogama, H., Fujimori, S., Hasegawa, T., Hayashi, M., Hirabayashi, Y., Ogura, T., Iizumi, T., Takahashi, K., Takemura, T., 2023. Important distinctiveness of SSP3–7.0 for use in impact assessments. Nat. Clim. Chang. 13, 1276–1278.
Shuttleworth, W.J., 1993. Evaporation. In: Maidment, D.R. (Ed.), Handbook of Hydrology. McGraw-Hill Inc, New York, USA, p. 4.1.
Song, Z., Xia, J., Wang, G., She, D., Hu, C., Hong, S., 2022. Regionalization of hydrological model parameters using gradient boosting machine. Hydrol. Earth Syst. Sci. 26, 505–524.
Song, Z., Xia, J., Wang, G., She, D., Hu, C., Piao, S., 2023. Climate change rather than vegetation greening dominates runoff change in China. J Hydrol (amst) 129519.
Sun, G., Caldwell, P., Noormets, A., McNulty, S.G., Cohen, E., Moore Myers, J., Domec, J.-C., Treasure, E., Mu, Q., Xiao, J., John, R., Chen, J., 2011. Upscaling key ecosystem functions across the conterminous United States by a water-centric ecosystem model. J. Geophys. Res. 116, G00J05.
Sun, G., Caldwell, P.V., McNulty, S.G., 2015a. Modelling the potential role of forest thinning in maintaining water supplies under a changing climate across the conterminous United States. Hydrol. Process. 29, 5016–5030.
Sun, G., Liu, N., Cao, R., Jin, K., Hao, L., Song, C., 2023a. Modeling forest-water interactions at multiple scales in Nepal, in: Sun, G., Bruijnzeel, L.A., Zhang, J., Tiwari, K.R., Hao, L. (Eds.), Proceedings of the International Symposium on Forests-Water-Livelihood Nexus in the Lesser Himalaya. Institute of Forestry, Tribhuvan University, Pokhara, Nepal, pp. 48–49.
Sun, G., McNulty, S.G., Moore Myers, J.A., Cohen, E.C., 2008. Impacts of Multiple Stresses on Water Demand and Supply Across the Southeastern United States. JAWRA Journal of the American Water Resources Association 44, 1441–1457.
Sun, S., Sun, G., Caldwell, P., McNulty, S.G., Cohen, E., Xiao, J., Zhang, Y., 2015b. Drought impacts on ecosystem functions of the U.S. National Forests and Grasslands: Part I evaluation of a water and carbon balance model. For. Ecol. Manage. 353, 260–268.
Sun, S., Sun, G., Cohen, E., McNulty, S.G., Caldwell, P.V., Duan, K., Zhang, Y., 2016. Projecting water yield and ecosystem productivity across the United States by linking an ecohydrological model to WRF dynamically downscaled climate data. Hydrol. Earth Syst. Sci. 20, 935–952.
Sun, G., Tiwari, K.R., Hao, L., Amatya, D., Liu, N., Song, C., 2023b. Climate change and forest hydrology in future forests. In: McNulty, S.G. (Ed.), Future Forests: Mitigation and Adaptation to Climate Change. Elsevier, Cambridge, MA, United States, pp. 95–124.
Teng, H., Chen, S., Hu, B., Shi, Z., 2023. Future changes and driving factors of global peak vegetation growth based on CMIP6 simulations. Ecol Inform 75, 102031.
Thornthwaite, C.W., 1948. An Approach toward a Rational Classification of Climate. Geogr. Rev. 38, 55–94.
Usbr, 2013. Downscaled CMIP3 and CMIP5 climate projections: Release of downscaled CMIP5 climate projections, comparison with preceding information, and summary of user needs. USA, U.S, Department of the Interior, Bureau of Reclamation, Technical Service Center, Denver.

USGS, 2011. National Land Cover Database (NLCD) 2006 land cover conterminous United States, U.S. Geological Survey data release [WWW Document]. https://doi.org/10.5066/P9HBR9V3.

Voldoire, A., Sanchez-Gomez, E., Salas y Mélia, D., Decharme, B., Cassou, C., Sénési, S., Valcke, S., Beau, I., Alias, A., Chevallier, M., Déqué, M., Deshayes, J., Douville, H., Fernandez, E., Madec, G., Maisonnave, E., Moine, M.-P., Planton, S., Saint-Martin, D., Szopa, S., Tyteca, S., Alkama, R., Belamari, S., Braun, A., Coquart, L., Chauvin, F., 2013. The CNRM-CM5.1 global climate model: description and basic evaluation. Clim Dyn 40, 2091–2121. https://doi.org/10.1007/s00382-011-1259-y.

Volodin, E.M., Dianskii, N.A., Gusev, A.V., 2010. Simulating present-day climate with the INMCM4.0 coupled model of the atmospheric and oceanic general circulations. Izv. Atmos. Ocean. Phys. 46, 414–431.

Wang, H., Lv, X., Zhang, M., 2021. Sensitivity and attribution analysis based on the Budyko hypothesis for streamflow change in the Baiyangdian catchment. China. Ecol Indic 121, 107221.

Warziniack, T., Arabi, M., Brown, T.C., Froemke, P., Ghosh, R., Rasmussen, S., Swartzentruber, R., 2022. Projections of Freshwater Use in the United States Under Climate Change. Earths Future 10.

Watanabe, M., Suzuki, T., O'ishi, R., Komuro, Y., Watanabe, S., Emori, S., Takemura, T., Chikira, M., Ogura, T., Sekiguchi, M., Takata, K., Yamazaki, D., Yokohata, T., Nozawa, T., Hasumi, H., Tatebe, H., Kimoto, M., 2010. Improved Climate Simulation by MIROC5: Mean States, Variability, and Climate Sensitivity. J Clim 23, 6312–6335.

Watanabe, S., Hajima, T., Sudo, K., Nagashima, T., Takemura, T., Okajima, H., Nozawa, T., Kawase, H., Abe, M., Yokohata, T., Ise, T., Sato, H., Kato, E., Takata, K., Emori, S., Kawamiya, M., 2011. MIROC-ESM 2010: model description and basic results of CMIP5-20c3m experiments. Geosci. Model Dev. 4, 845–872.

Wuebbles, D., Meehl, G., Hayhoe, K., Karl, T.R., Kunkel, K., Santer, B., Wehner, M., Colle, B., Fischer, E.M., Fu, R., Goodman, A., Janssen, E., Kharin, V., Lee, H., Li, W., Long, L.N., Olsen, S.C., Pan, Z., Seth, A., Sheffield, J., Sun, L., 2014. CMIP5 Climate Model Analyses: Climate Extremes in the United States. Bull. Am. Meteorol. Soc. 95, 571–583.

Yang, Y., Roderick, M.L., Guo, H., Miralles, D.G., Zhang, L., Fatichi, S., Luo, X., Zhang, Y., McVicar, T.R., Tu, Z., Keenan, T.F., Fisher, J.B., Gan, R., Zhang, X., Piao, S., Zhang, B., Yang, D., 2023. Evapotranspiration on a greening Earth. Nat Rev Earth Environ 4, 626–641.

Yukimoto, S., Adachi, Y., Hosaka, M., Sakami, T., Yoshimura, H., Hirabara, M., Tanaka, T.Y., Shindo, E., Tsujino, H., Deushi, M., Mizuta, R., Yabu, S., Obata, A., Nakano, H., Koshiro, T., Ose, T., Kitoh, A., 2012. A New Global Climate Model of the Meteorological Research Institute: MRI-CGCM3 —Model Description and Basic Performance—. Journal of the Meteorological Society of Japan. Ser. II 90A, 23–64.

Zhang, L., Dawes, W.R., Walker, G.R., 2001. Response of mean annual evapotranspiration to vegetation changes at catchment scale. Water Resour. Res. 37, 701–708.

Zhang, Y., Li, C., Chiew, F.H.S., Post, D.A., Zhang, X., Ma, N., Tian, J., Kong, D., Leung, L. R., Yu, Q., Shi, J., Liu, C., 2023. Southern Hemisphere dominates recent decline in global water availability. Science 1979 (382), 579–584.

Zhang, M., Liu, N., Harper, R., Li, Q., Liu, K., Wei, X., Ning, D., Hou, Y., Liu, S., 2017. A global review on hydrological responses to forest change across multiple spatial scales: Importance of scale, climate, forest type and hydrological regime. J Hydrol (amst) 546, 44–59.

Zhang, G., Wu, Y., Li, H., Yin, X., Chervan, A., Liu, S., Qiu, L., Zhao, F., Sun, P., Wang, W., Jin, Z., 2024. Assessment framework of water conservation based on analytical modeling of ecohydrological processes. J Hydrol (amst) 630, 130646.

Zhao, M., Heinsch, F.A., Nemani, R.R., Running, S.W., 2005. Improvements of the MODIS terrestrial gross and net primary production global data set. Remote Sens. Environ. 95, 164–176.

Zhou, D., Hao, L., Kim, J.B., Liu, P., Pan, C., Liu, Y., Sun, G., 2019. Potential impacts of climate change on vegetation dynamics and ecosystem function in a mountain watershed on the Qinghai-Tibet Plateau. Clim. Change 156, 31–50.

Zhou, S., Yu, B., Lintner, B.R., Findell, K.L., Zhang, Y., 2023. Projected increase in global runoff dominated by land surface changes. Nat. Clim. Chang.